Revised version sent to JGR
21 July 1999

The origin of the near-Earth plasma population during a substorm on November 24, 1996

M. Ashour-Abdalla, M. El-Alaoui, V. Peroomian, R. J. Walker, J. Raeder

Institute of Geophysics and Planetary Physics, UCLA

L. A. Frank, W. R. Paterson

Department of Physics and Astronomy, University of Iowa

Abstract. We investigate the origins and the transport of ions observed in the near-Earth plasma sheet during the growth and expansion phases of a magnetospheric substorm that occurred on November 24, 1996. Ions observed at Geotail were traced backward in time in time-dependent magnetic and electric fields to determine their origins and the acceleration mechanisms responsible for their energization. Results from this investigation indicate that, during the growth phase of the substorm, most of the ions reaching Geotail had origins in the low latitude boundary layer (LLBL) and had already entered the magnetosphere when the growth phase began. Late in the growth phase and in the expansion phase a higher proportion of the ions reaching Geotail had their origin in the plasma mantle. Indeed, during the expansion phase more than 90% of the ions seen by Geotail were from the mantle. The ions were accelerated enroute to the spacecraft; however, most of the ions' energy gain was achieved by non-adiabatic acceleration while crossing the equatorial current sheet just prior to their detection by Geotail. In general, the plasma mantle from both southern and northern hemispheres supplied non-adiabatic ions to Geotail, whereas the LLBL supplied mostly adiabatic ions to the distributions measured by the spacecraft. Distribution functions computed at the ion sources indicate that ionospheric

ions reaching Geotail during the expansion phase were significantly heated. Plasma mantle source distributions indicated the presence of a high-latitude reconnection region that allowed ion entry into the magnetosphere when the IMF was northward. These ions reached Geotail during the expansion phase. Ions from the traditional plasma mantle had access to the spacecraft throughout the substorm.

1. Introduction

It has long been established that the state of the Earth's magnetosphere is strongly affected by the orientation of the interplanetary magnetic field (IMF) and by the dynamics of the solar wind. During intervals of southward IMF, magnetic reconnection occurs at the dayside magnetopause [e. g. *Cowley*, 1980], causing the electric field in the solar wind to be conducted towards the high-latitude magnetosphere and into the geomagnetic tail. During northward IMF, high-latitude reconnection poleward of the polar cusp strongly influences the magnetospheric configuration [*Song and Russell*, 1992 and references therein]. The transport of mass, momentum and energy from the solar wind into the magnetosphere through the plasma mantle and the LLBL, as well as the role of the ionosphere in populating the near-Earth tail are not well understood.

In an effort to understand this transport, numerous studies have been carried out on the population of the quiet-time magnetotail from the solar wind, the ionosphere, or a combination of both. Following the observations of energetic O^+ ions precipitating into the ionosphere [*Shelley et al.*, 1972], investigations established that the auroral zone and the cleft ion fountain are robust sources of ions for the near-Earth magnetotail [e.g., *Yau et al.*, 1985; *Lockwood et al.*, 1985a, b].

Solar wind ions, on the other hand, were found to enter the magnetosphere through the plasma mantle and the low latitude boundary layer (LLBL) in adequate numbers to populate the entire magnetotail [*Pilipp and Morfill*, 1978; *Mitchell et al.*, 1987]. By using O^+ and He^{++} ions as tracers of ionospheric and solar wind ion populations, many studies have confirmed that both the solar wind and the ionosphere contribute to the magnetospheric plasma population [*Eastman et al.*, 1976; *Lennartsson and Shelley,* 1986; *Chappell et al.*, 1987; *Lennartsson*, 1992]. Based on their finding of a direct correlation between solar wind and plasma sheet ion densities, *Borovsky et al.* [1997] argued that the magnetotail ion population is principally composed of solar wind particles. In contrast, advocates of the "Geopause" [*Moore*, 1991; *Moore and Delcourt*, 1995; *Winglee*, 1998] argued that a boundary exists earthward of which the ion population is dominated by ionospheric particles. *Winglee* [1998] used a multi-fluid magnetohydrodynamic (MHD) simulation to show that the geopause could extend beyond $x = -50\ R_E$ for certain orientations of the IMF.

Theoretical studies of the population of the magnetotail generally focus on a single source region and attempt to gauge the importance of that region in the population of the tail. By using a Monte Carlo diffusion code, *Cladis and Francis* [1985] showed that the polar ionosphere is a viable source of storm-time ring current ions. Phase bunching in ion distributions caused by a violation of the second adiabatic invariant were examined by *Mauk* [1986]. Later, *Delcourt et al.* [1995] examined phase bunching caused by the violation of the first adiabatic invariant. *Delcourt et al.* [1989, 1990] used the cleft ion fountain as a source to populate the plasma sheet during the growth and expansion phases of substorms. These studies are in agreement with observations of increased fluxes of ionospheric ions in the near-Earth tail during geomagnetically active (storm and substorm) periods [e.g. *Hamilton et al.*, 1988]

Starting from a plasma mantle source, *Ashour-Abdalla et al.* [1993, 1994, 1995] used a large-scale kinetic (LSK) orbit tracing technique and showed that the plasma sheet can be formed by the plasma mantle, and that the non-adiabatic acceleration of ions in the neutral sheet leads to the formation of thin current sheets, the occurrence of non-gyrotropic ion distributions, and off-diagonal terms in the pressure tensor. *Peroomian and Ashour-Abdalla* [1995, 1996] made a comparative study of the contribution of the solar wind and the ionosphere to near-Earth plasma populations and found that distinct regions in the equatorial magnetotail were dominated by ions from a given source. Namely, the mid-tail and dusk flanks were dominated by mantle ions, the dawn flanks by LLBL ions. *Peroomian and Ashour-Abdalla* found that the ring current was composed of a mixture of particles from all three sources.

Despite these studies, a number of processes involved in populating the magnetotail remain unclear. These include the role each source plays and how that role evolves during more active times or during substorms, the entry mechanism of ions into the magnetosphere, and the transport of plasma from each source to the near-Earth tail.

In order to answer some of the outstanding questions of plasma population and particle transport in the magnetotail, we have constructed a time-dependent large-scale kinetic (LSK) model that employs electric and magnetic fields from a global MHD simulation. Global MHD models of the magnetosphere have become increasingly complex, and as a result it is now possible to construct an accurate model of the magnetospheric configuration by using real-time observed solar wind and IMF parameters as input into the MHD models [*Frank et al.*, 1995; *Raeder et al.*, 1997; *Goodrich et al.*, 1998]. We have successfully applied our LSK technique to studying the non-Maxwellian features of near-Earth distribution functions measured by Geotail

during a quiet interval and to the evolution of ion sources during an extended period of northward IMF [*Ashour-Abdalla et al.*, 1997, 1999].

In this paper, we apply the time-dependent LSK technique to more active times and present a detailed analysis of the dynamics of ion transport in the near-Earth magnetotail during the November 24, 1996, substorm with the use of observations from the Geotail spacecraft, a time-dependent MHD model run with solar wind data from the WIND satellite, and time-dependent LSK calculations of ion orbits. By combining observations with MHD simulations and trajectory calculations, we can illuminate the physics underlying the explosive substorm process and gain a better understanding of the contribution of individual ion sources and their evolution as the substorm progresses.

Following this introduction, we summarize the observations of the November 24, 1996, substorm. Section 3 outlines the methodology used in this study. Section 4 presents our results: we discuss the MHD results, plasma entry into the magnetosphere, its transport and acceleration; finally, we calculate the velocity distribution functions at the ion source regions. Section 5 summarizes our findings.

2. Observations and Model

a. Observations

Early on November 24, 1996, the magnetosphere was relatively quiet. For the first 6 hours K_p was 0^+ and 1^-. Figure 1 shows the auroral electrojet indices calculated from the Canadian CANOPUS magnetometer chain, which was ideally situated to capture the onset of the substorm. Although the CANOPUS indices are not necessarily representative of the global auroral indices, they provide useful information about the local auroral dynamics and electrojet activity during the period of interest. The upper (lower) panel of Figure 1 shows the CU (CL) index, which is

the highest (lowest) value of the horizontal magnetic field at one-minute intervals. The CANOPUS data indicate that this substorm had multiple intensifications; the growth phase began at ~0730 UT and the expansion phase for the first intensification at ~0820 UT.

Figure 2 shows the solar wind and interplanetary magnetic field (IMF) observations from the WIND spacecraft for the period 0300 UT – 1000 UT. During this interval WIND was located upstream of the Earth at (72.4, –20.7, 8.06) R_E. The panels in this plot are, from top to bottom, the three components of the interplanetary magnetic field (IMF) (in nT), the three components of solar wind velocity (in km/s), the solar wind plasma density (in cm^{-3}) and the plasma pressure (in pPa). The IMF data show that B_z was predominantly northward prior to substorm onset and turned southward at ~ 0700 UT. The B_x and B_y components of the IMF were both small during this interval. However, the B_y component showed a significant negative turning that coincided with the southward turning of the B_z component. The solar wind velocity was steady and predominantly in the x direction with an average speed of ~310 km/s, placing the WIND spacecraft approximately 25 minutes upstream of Earth. The plasma density at the beginning of the interval was much higher than average, ~20 cm^{-3}, and increased steadily, reaching ~35 cm^{-3} during the substorm. The increase in density was mirrored in the solar wind plasma pressure profile, which increased from ~ 6 pPa to over 30 pPa during the substorm. The increases in density and pressure began to occur at the same time as the southward turning of the IMF, and reached their peak values at ~0800 UT.

During the November 24, 1996 substorm the Geotail spacecraft was located in the near-midnight magnetotail about 21 R_E from the Earth. (Geotail moved from (–20.7, 2.8, –2.3) R_E to (–21.5, 1.7, –2.4) R_E during the substorm.) Three-dimensional ion distribution functions (Figure 3) from the Hot Plasma analyzer (HP) of the Comprehensive Plasma Instrumentation (CPI) on Geotail [*Frank et al.*, 1994] reveal a very complex structure. For the observations presented here, the HP analyzer was operated in a mode in which the ion velocity distributions were determined, with more than 3000 samples falling within the energy-per-unit charge (E/Q) range of 22 V to 48 kV with a repetition rate of 22 s. The distribution functions shown in Figure 3 are averaged over 64 seconds. The limitations of the instruments on board Geotail are well known. However, the spacecraft carries two ion instruments that are complimentary in nature, the LEP and the CPI. The former has good time resolution and a large geometric factor and the latter has better

resolution in phase space. Since the purpose of this study was to gain insight into the dynamics of the magnetotail and to ascertain the entry mechanisms and transport processes during a magnetospheric substorm, it was necessary to use the instrument with better phase space resolution, that is CPI. For this interval, the plasma moments obtained from the two instruments are nearly identical, giving us confidence in the measured distribution functions.

In Figure 3 the distribution function is plotted in V_y - V_z,, V_x - V_z, and V_x - V_y projections in GSE coordinates. The six rows give the distribution functions at 0740 UT, 0750 UT, 0800 UT, and 0810 UT during the growth phase and at 0830 UT and 0840 UT during the expansion phase. The projection of the average magnetic field vector is superimposed over each of the distribution functions. At 0740 UT the magnetic field was mainly tailward and strong earthward field-aligned flows existed, signs that Geotail was located in the southern plasma sheet boundary layer (PSBL). Thereafter, Geotail moved deeper into the plasma sheet, as indicated by the hotter, earthward convecting distribution measured by the spacecraft at 0750 UT. At 0800 UT, in the middle of the growth phase, the distribution function became much colder. Geotail magnetic field measurements shown in Figure 4 indicate that the spacecraft may have briefly entered the northern PSBL or lobe region during this interval. At 0810 UT, the Geotail distribution is dominated by an earthward flowing beam. Figure 3 also shows evidence of a counter-streaming beam-like component. At 0830 UT, Geotail has once again moved closer to the PSBL/lobe boundary as evidenced in the cold distribution measured at this time. Finally, at 0840 UT, Geotail moved to the outer edge of the PSBL and observed mostly cold plasma convecting equatorward into the plasma sheet. We note that despite the differences in the six distribution functions shown in Figure 3, one feature is common to all: all six distributions exhibit a large amount of structuring. The goal of this study is to understand the sources of the plasmas observed in Figure 3.

In order to ascertain Geotail's location with respect to magnetospheric boundaries during these six intervals, we plot in Figure 4 the three components of the magnetic field measured by the magnetic field experiment (MFE) on Geotail [*Kokubun et al.*, 1994] and the x-component of the bulk velocity as measured by CPI/HP (solid curves in Figure 4). Prior to 0735 UT, Geotail was located in the southern lobe. The beginning of the growth phase, as indicated by the increase in the westward electrojet at CANOPUS (Figure 1), occurred just before 0740 UT. At this time, the magnetic field was mainly tailward and strong earthward field-aligned flows

existed, signs that Geotail was located in the southern plasma sheet boundary layer (PSBL). Thereafter, Geotail moved deeper into the plasma sheet, as indicated by the larger B_Z and the earthward convection found ten minutes later (at 0750 UT). By 0800 UT, near the end of the growth phase the distribution function was much colder and the magnetic field pointed predominantly earthward, from which we conclude that Geotail was near the northern boundary of the plasma sheet. At 0810 UT and 0830 UT, Geotail was in the northern PSBL, interrupted at ~0816 UT by a brief excursion back into the current sheet. Finally at 0840 UT Geotail moved to the outer edge of the northern plasma sheet boundary layer and observed mostly cold plasma convecting equatorward into the plasma sheet. Because Geotail moved into the northern lobe shortly after 0845 UT, we concentrate our efforts on the growth phase and the first intensification of this substorm. The dotted curves in Figure 4 indicate the results obtained from the global MHD simulation at the Geotail location and will be discussed in the next subsection.

b. The MHD Model

This study investigates ion transport through the magnetosphere by tracing the trajectories of thousands of particles in time-dependent electric and magnetic fields obtained from a global MHD simulation of the November 24, 1996, substorm. The MHD model essentially solves the ideal MHD equations that are modified to include an anomalous resistivity term for the magnetosphere and a potential equation for the ionosphere. A few numerical effects, such as diffusion, viscosity, and resistivity, are necessarily introduced by the numerical methods. These permit viscous interactions and, to a limited extent, magnetic field reconnection. However, the numerical scheme is optimized to minimize numerical effects. For instance, numerical resistivity is so low that it is necessary to introduce an anomalous resistivity term in order to model substorms correctly [see *Raeder et al.*, 1995, 1996]. The ionospheric part of the model takes into account three sources of ionospheric conductance: solar EUV ionization is modeled by using the empirical model of *Moen and Brekke* [1993], diffuse auroral precipitation is modeled by assuming strong pitch angle scattering at the inner boundary of the MHD simulation (at 3.7 R_E), and accelerated electron precipitation associated with upward field-aligned currents is modeled in accordance with the approach of *Knight* [1972] and *Lyons et al.* [1979]. The empirical formulas of *Robinson et al.* [1987] are used to calculate the ionospheric conductances from the

electron mean energies and the energy fluxes. A detailed description of the MHD model, including initial and boundary conditions, can be found in *Raeder et al.* [1996, 1997].
The electric field used in this calculation is given by $\mathbf{E} = -\mathbf{V} \times \mathbf{B} + \eta\mathbf{J}$, where **V** is the velocity from the MHD model, **B** is the magnetic field, η is the resistivity, and **J** is the current density. The electric field has both a convective ($-\mathbf{V} \times \mathbf{B}$) and a resistive ($\eta\mathbf{J}$) term. The resistive term becomes important near the magnetopause and near x-lines but is negligible elsewhere.

The solar wind observations shown in Figure 2 were used as input to the global MHD code. Before 0700 UT, the IMF had a northward z component. The southward IMF observed by WIND at 0700 UT reached the magnetopause at about 0725 UT, causing the reconnection site to move from the high-latitude magnetopause to the subsolar magnetopause. The predominantly duskward B_y component of the IMF during the four hours prior to the southward turning caused the magnetotail to rotate such that the plasma sheet was north of the $z = 0$ plane on the dusk side of the tail and south of it on the dawn side. This placed the simulated Geotail location in the southern PSBL during the early growth phase of the substorm, as was observed (dotted curves in Figure 4). By 0750 UT the duskside plasma sheet near Geotail began to rotate in response to the dawnward rotation of the IMF, and the spacecraft moved toward the center of the plasma sheet in both the observations and the simulation. The comparison between the simulation results (dotted curves) and Geotail observations (solid curves) shown in Figure 4 are generally good. However, the MHD simulation used in this paper is far from ideal. When using a single point measurement of the solar wind ~80 R_E upstream of Earth, it is not possible to compensate for structures in the solar wind. For example, structures measured by the Wind spacecraft and used as input for our simulations may never encounter Earth and this results in discrepancies between the model and observations. At the same time, the spatial grid used in the simulation is often too coarse to resolve sharp gradients (both temporal and spatial) in plasma and magnetic field parameters. Also, we use a simple model for the B_x in our simulations and hold Earth's dipole tilt constant throughout the simulation. Both of these approximations can lead to errors, especially late in the simulation run. Despite these shortcomings we chose to use MHD simulations simply because they are the best global models available for our purposes. MHD simulations using upstream satellite data as input have reproduced the global features remarkably well, including the magnetic field topology, of the magnetosphere [*Frank et al.*, 1995; *Raeder et al.*, 1997; *Berchem et al.*, 1998a,b; *Goodrich et al.*, 1998; Ashour-Abdalla et al., 1998, 1999]. A detailed

comparison and analysis of the dynamics of the plasma sheet at the Geotail location will appear in *El-Alaoui* [1999]. Figure 5 shows the pressure in the $x - z$ (left-hand column) and $y - z$ (right-hand column) planes through the location of Geotail during the substorm. At 0800 UT (Figures 5a and 5b), during the growth phase of the substorm, Geotail was in the plasma sheet. A thin current sheet formed and extended tailward of Geotail. At 0830 UT (Figures 5c and 5d), early in the expansion phase, reconnection was occurring tailward of the spacecraft. Following the onset of reconnection, the plasma sheet earthward of Geotail thickened (compare the 0830 UT plasma sheet distribution with that at 0902 UT in Figure 5e). At the same time the entire duskside plasma sheet continued to move southward in response to the dawnward turning of the IMF ($B_y < 0$). The net effect of these movements was to place Geotail in the northern plasma sheet boundary layer during the expansion phase of the substorm. These changes caused significant variations in the ion distributions measured at Geotail. We discuss these changes below.

Another feature affecting ion entry into the magnetosphere is the occurrence of reconnection at the magnetopause. Figure 6 shows two snapshots of magnetic field lines in the MHD model at t = 0700 UT (top panel), when the IMF was northward, and at 0800 UT (bottom panel), after the IMF had turned southward . During northward IMF, reconnection occurrs at high latitudes in the MHD model (shown by arrow in Figure 6a). Later, when the IMF turs southward, the reconnection site shifts to the dayside (shown by arrow in Figure 6b). As we will discuss below in section 4c, this feature causes significant changes in ion entry into the magnetosphere and has a signature that can be discerned by examining the ions measured at Geotail.

3. Methodology

We construct three-dimensional distribution functions in velocity space representative of the Geotail distribution functions shown in Figure 3 by placing ~75,000 ions in V_x - V_y - V_z bins (100 km/s × 100 km/s × 100 km/s) such that the number in each bin is proportional to the phase space density observed at the Geotail spacecraft. One particle in the computational distribution function corresponds to 5×10^{-27} s^3cm^{-6} in the Geotail distribution function. Since we use a large number of test particles per distribution, we populate the densest part of the distribution

with more than 1000 particles per bin, and the lowest contour level of the distributions shown in Figure 3 by at least 10 particles per bin. Moreover, particles in each velocity bin are randomized in phase space within that bin to assure complete coverage of phase space in each bin. Since we start with the three-dimensional velocity vectors measured by Geotail, this process assures that we have complete coverage of the phase space measured by the spacecraft. Because the magnetospheric topology, especially near the magnetopause and the magnetotail current sheet, causes ions to behave nonadiabatically and to violate the conservation of the first adiabatic invariant [*Speiser*, 1965; *Lyons and Speiser*, 1982; *Chen and Palmadesso*, 1986; *Büchner and Zelenyi*, 1986, 1989] it is necessary to follow the exact motion of ions. Therefore, for each particle we integrate the equation of motion ($d\mathbf{V}/dt = q\mathbf{V} \times \mathbf{B}+q\mathbf{E}$) backward in time until the particle encounters the magnetopause (as defined by the current distribution in the MHD model), the ionosphere (taken as the inner boundary of the MHD simulation at $r = 4.0\ R_E$), or the tailward edge of the simulation box, placed at $x = -150\ R_E$. Since the minimum grid spacing in the global MHD model is relatively large ($\sim 0.25 - 0.5\ R_E$) and the simulation data are saved at four-minute time intervals, we use linear interpolation in both space and time to determine the instantaneous values of the MHD fields on scales smaller than the grid spacing. We use a fourth-order Runge-Kutta method to calculate the ion trajectories in the evolving magnetic and electric fields. The time step for the particle trajectory calculation is nominally set at 0.002 times the local ion gyro-period, with an upper limit imposed to ensure that the time step does not get too large in weak field regions. This ensures that all the particles in the simulation conserve energy (to 6 significant figures) and that the trajectory is calculated correctly in the model. The exact method for calculating particle trajectories insures that the particles' phase information is preserved even through the non-adiabatic regions. This is of primary importance when tracing particles in a narrow loss cone back into the ionosphere. In fact, because our ionospheric boundary is set at a radial distance of $4.0\ R_E$, our resultant "loss cone" is larger than the real loss cone at Geotail. Previously, we have shown that up to 40% of ions from a Geotail distribution measured in the near-Earth ($x \sim -10\ R_E$) tail originate in the ionosphere [*Ashour-Abdalla et al.*, 1997]. Our methodology for the backward tracing of particles is further borne out by our results discussed in section 4c, where ionospheric ions are found to originate from 2 beams in the northern nightside auroral zone and a conic-like heated structure from the southern dayside cusp region, indicating that we can resolve detailed structures in the ionospheric source region.

4. Results

Our study analyzed four intervals during the growth phase and two intervals during the expansion phase of the substorm; we discuss our findings here. Tracing ions from the Geotail distribution functions shown in Figure 3 backward to their point of origin reveals a great deal about the evolution of plasma sources for the near-Earth tail, the transport and acceleration mechanisms operating during the substorm, and the evolution of distribution functions at the source regions supplying the Geotail spacecraft.

a. Plasma Entry into the Magnetosphere

Figure 7 shows the point where ions observed at Geotail enter the magnetosphere. Each color-coded dot in the figure represents the number of ions originating from a 1 $R_E \times 1$ $R_E \times 1$ R_E region centered at the point. As discussed in section 3, we obtain the information plotted in Figure 7 by tracing ions backward from the Geotail distributions to their source regions. The green sphere shows the location of Geotail, and the contour plot in each panel represents a profile of the plasma pressure at $x = -150$ R_E at the time of measurement. Most (84%) of the ions observed at Geotail at 0740 (Figure 7a) during the growth phase of the substorm enter the magnetosphere at low latitudes in the dusk flank. These ions enter the magnetosphere prior to the beginning of the growth phase. About 14% of the ions enter the magnetosphere in the distant ($x < -100$ R_E) plasma mantle. These ions originate on IMF field lines that reconnected on the dayside and were swept downtail. Because of their original motion "down" the IMF field line, these ions are found to be primarily field aligned and moving earthward. They are responsible for the earthward streaming component seen at Geotail. Thus, we distinguish between LLBL and mantle particles by their method of entry into the magnetosphere, rather than by traditional boundaries drawn for static and non-twisted magnetospheric configurations. Ionospheric ions make up < 1% of the population at Geotail at this time.

Ten minutes later, at 0750 UT (Figure 7b), the LLBL is still the dominant source of ions (82%), with the bulk of this plasma flowing perpendicular to the magnetic field (as ascertained from examining individual ion orbits). Dayside reconnection has enhanced the region from

which mantle ions can reach Geotail. The plasma mantle now supplies ~17% of the ions at Geotail, most of which are concentrated in a heated earthward flowing beam (second row of Figure 3). The ionospheric contribution at this time is still negligible. At 0800 UT the plasma mantle has become a significant (~37%) source of ions in the near-Earth tail (Figure 7c).

The formation of a near-Earth neutral line is followed closely by the formation of a flux rope in the tail. Evidence of this can be seen in Figure 7d, which shows the entry points for 0810 UT. Here, the dusk flank of the magnetosphere is populated by IMF field lines (magenta). This change in magnetospheric configuration has a significant impact on the access ions have to the Geotail location. Figure 7d shows that the LLBL source has diminished greatly and is supplying only 9% of the ions at Geotail. Particles entering the magnetosphere in this region are swept downtail by a tailward flow generated by the near-Earth neutral line. In fact, only LLBL ions that have entered the magnetosphere prior to the beginning of the growth phase make it to the spacecraft. The northern plasma mantle is the dominant source (providing 68% of the ions at Geotail), followed by plasma mantle ions from the southern hemisphere (21% of the ions), which reach Geotail for the first time during the substorm. In sharp contrast to the previous intervals, more than 65% of the ions reaching Geotail at 0810 UT do so from beyond 150 R_E downtail (the tailward limit of our simulation box), further evidence of the stretching of open field lines during this phase of the substorm.

0830 UT coincides with the formation and ejection of the plasmoid in the magnetotail. Because of this, very few LLBL ions reach the spacecraft. Also, more than 83% of the ions reaching Geotail do so from beyond 150 R_E downtail (Figure 7e).

By 0840 UT, the magnetotail has reached an expansion phase configuration in which IMF field lines formed by the reconnection of lobe field lines extend downtail from the near-Earth neutral line and lobe field lines are stretched far downtail (Figure 7f). At this time, the plasma mantle source from both hemispheres has moved much closer to the spacecraft. Together, the northern and southern mantle sources supply about 90% of the ions seen at Geotail. LLBL ions constitute 10% of the particles seen at Geotail, and the ionospheric source contributes ~ 2% of the ions at the spacecraft (Figure 7f). The northern plasma mantle ions enter the magnetosphere from a broad region extending tailward from $x = -30\ R_E$. The number density of ions entering through this region shows two localized peaks in the near-Earth and far-tail regions (shown by arrows in Figure 7f). We consider this feature in detail in section 4c below.

The six intervals examined here show that the dynamic changes occurring during the substorm alter the ability of plasma sources to reach the near-Earth region. This is partly caused by changes in magnetic field line topology. Figure 8 plots the percentage of ions measured at Geotail that originate from the three sources identified in Figure 7 (northern+southern plasma mantle, LLBL, and the ionosphere). Figure 8 indicates that the plasma mantle contribution to the plasma measured at Geotail increases as a function of time with a corresponding decrease in LLBL contribution. The ionospheric contribution grows fomr < 1% to just over 2.5% during the expansion phase of the substorm. We note that at 0830 UT, more than 80% of ions reaching Geotail do so from beyond x = -150 R_E downtail (the downtail boundary of our test particle runs). Accordingly, the percentages shown in Figure 8 for 0830 UT are calculated only for the fraction of ions for which we have definite source information. In the next subsection, we examine the acceleration mechanisms operating inside the magnetosphere to gain a better understanding of internal processes taking place during the substorm.

b. Transport and Acceleration of Plasma

The paths that ions from each source follow to Geotail are as varied as the locations of the sources supplying ions to the spacecraft. Figure 9 shows the trajectory of a duskside LLBL ion detected by Geotail at 0750 UT. The three panels show, from top to bottom, the $x - z$ projection of the ion's orbit, the $x - y$ projection of the orbit, and the ion's kinetic energy (black curve, scale on left) and parameter of adiabaticity κ [*Büchner and Zelenyi*, 1989] (red dots, scale on right, shown only when $\kappa < 5$) as a function of time. Early in the ion's orbit, $\kappa > 5$; these values are not shown in the lower panel of Figure 9. Plasma in the LLBL flows in an anti-sunward direction [*Eastman and Hones*, 1979]. Accordingly, the ion shown in Figure 9 enters the magnetosphere at x ~ –90 R_E in the dusk flank and is swept downtail before convecting onto a closed field line at x ~ –130 R_E and returning earthward. After mirror-bouncing near Earth, and about 1.8 hours after entering the magnetosphere, the ion is detected by Geotail. The bottom panel of Figure 9 shows that the ion enters the magnetosphere with ~ 500 eV energy, and gains very little energy until just before reaching Geotail. There, it interacts with the current sheet and gains ~ 4 keV of energy in a short period of time. This occurs because, for the first time during the orbit, $\kappa < 1$ (see red dots in bottom panel of Figure 9) allowing the ion to undergo nonadiabatic acceleration.

Plasma mantle ions enter the magnetosphere on field lines that reconnected on the dayside and were swept downtail [*Pilipp and Morfill*, 1978]. Figure 10 shows one such ion as it begins its earthward convection from just inside the topside magnetopause at $x \sim -65\ R_E$. As was the case with the LLBL ion (Figure 9), this ion also interacts with the current sheet and reaches Geotail with an energy slightly greater than 1 keV. In contrast to the LLBL particle, however, this ion reaches Geotail in only 40 minutes.

Another source of ions for Geotail is the ionosphere. Although this source supplies only ~ 2% of the ions to Geotail, the ionosphere is known to play a significant role in the later stages of substorms [*Lennartsson and Shelley*, 1986]. Figure 11 shows the orbit of an ion from the nightside auroral zone that reaches Geotail at 0840 UT. As is discussed in section 4c below, this ion is part of a 1 keV beam that reaches the spacecraft. Again, this ion is energized in the current sheet. More significant, however, is the lack of change in the ion's energy during the field-aligned portion of its orbit (before ~0838 UT), indicating the absence of parallel electric fields in the MHD model between r = 4 R_E and the spacecraft location.

Because of the spacecraft's location, many of the ions reaching Geotail experience nonadiabatic acceleration in the thin current sheet just tailward of the spacecraft. Table 1 shows a summary of the percentage of nonadiabatic ions reaching Geotail during the six intervals considered here. Clearly, the percentage of nonadiabatic ions is highest when the spacecraft is in the CPS. However, the onset of the expansion phase and the reconfiguration of field lines associated with it cause a significant drop in the percentage of ions that reach Geotail after being nonadiabatically accelerated. Figure 12 shows the entry points of ions for the 0800 UT and 0840 UT intervals in a format similar to Figure 7. Here, however, the color coding corresponds to the percentage of ions in each 1 R_E^3 bin that experience nonadiabatic acceleration during their orbits. Ion orbits were deemed to be nonadiabatic if the κ parameter dropped below 2 for any part of the ion orbit [see discussion by *Büchner and Zelenyi*, 1989 and by *Sergeev and Gvozdevsky*, 1995]. At 0800 UT (Figure 12a), the two major sources of ions, the LLBL and the plasma mantle, are clearly separated by κ. The LLBL ions are mostly adiabatic, while nearly all plasma mantle ions are nonadiabatic. The closed field lines in the tail (shown in red) are stretched, resulting in a large region where ions can violate the conservation of the magnetic moment μ. At 0840 UT (Figure 12b), however, the region previously containing stretched field lines is now in a region of open or IMF field lines formed by reconnection. The closed field lines have dipolarized, and

as a result the region where ions are nonadiabatic has contracted. Therefore, only a small portion of plasma mantle ions from both hemispheres is nonadiabatic.

Thus far, we have discussed the entry, acceleration, and transport of plasma during the November 24, 1996, substorm. Next, we examine the significant differences in the transit times for ions to move from the source regions to the Geotail location. Figure 13 shows the $x - z$ projection of the entry points for all six intervals, color coded according to the time of flight from entry to detection. At 0740 UT (Figure 13a), the LLBL population, on average, reaches Geotail after ~ 1 hour. In contrast, the mantle ions reach the spacecraft in less than 30 minutes. This difference is caused by the mantle ions' direct access along open field lines to Geotail. During the rest of the growth phase, at 0750 UT, 0800 UT, and 0810 UT, when the mantle source expands earthward, the transit times of the mantle source decrease downtail. This is because the increased distance from the spacecraft acts as a velocity filter, such that the energy of mantle ions with access to the spacecraft location increases downtail. Thus, only the low energy part of the distribution from the near-Earth mantle and only the high-energy portion from the distant mantle can reach Geotail.

Figure 7 shows that the formation of the flux rope and the ejection of the plasmoid downtail caused ions from the LLBL to lose access to the spacecraft location. Figure 13e shows that in fact, at 0830 UT, the transit times of LLBL ions to the spacecraft have increased dramatically. In other words, only slow LLBL ions that were inside the magnetosphere long before the formation of the flux rope have access to the spacecraft location.

The reconfiguration of the magnetotail is complete by 0840 UT. Once again, ions from both the northern and southern plasma mantles show the velocity filter effect. However, an additional population of northern mantle ions with very long transit times reaches Geotail from $x \sim -30\ R_E$ to $x \sim -50\ R_E$. We examine this effect in detail in section 4c.

c. Source Distributions

We construct source distribution functions by using the data from the entry points of ions (shown in Figure 7) and Liouville's theorem. This procedure maps the phase space density of the Geotail distribution onto the magnetopause and the ionosphere. It is then straightforward to calculate distribution functions at the source regions. We reproduce only the part of the source

distribution that reached Geotail, and not the entire source distribution. In this section, we discuss three significant features of velocity distributions calculated at the source regions.

As noted above, the formation of the flux rope hindered the ability of duskside LLBL ions to reach the spacecraft, and, as a result, the transit time from this source to the spacecraft increased. Figure 14 shows the $V_x - V_z$ projection of the LLBL distribution function at 0740 UT, 0800 UT, and 0830 UT. While the LLBL distribution is relatively cold for all three intervals, the temperature of the distribution of ions reaching Geotail from this source decreases from ~450 eV to less than 200 eV between 0740 UT and 0830 UT. This is consistent with the increase in the transit time of LLBL ions during the expansion phase.

Throughout the substorm both hemispheres of the ionosphere contribute a small number of particles to Geotail. However, the portion of the ionospheric distribution reaching Geotail increases significantly between the growth and expansion phases of the substorm. Figure 15 shows $V_{||} - V_{\perp}$ distribution functions calculated at the ionospheric source at 0740 UT during the growth phase (Figure 15a), and at 0840 UT during the expansion phase (Figure 15b). Throughout the growth phase, the portion of ionospheric outflow reaching Geotail is represented by a cold (~ 600 eV) distribution of ions upwelling from the region. Figure 15b shows that ions reaching Geotail have beam-like distributions at 0840 UT. Ions from the northern hemisphere form two beams with energies of 900 eV and 2.1 keV (labeled by 1 and 2 in Figure 15b) originating 1° apart in the nightside auroral zone (from projecting the data in Figure 15b onto the ionosphere). The energy of ions reaching Geotail from the southern hemisphere is much higher. The majority of these ions form a conic-like structure with an average energy of 4.3 keV. This corresponds to an average potential drop of 1.4 kV/R_E (0.22 mV/m) between the ionosphere and the point where the distribution was calculated at $r = 4\ R_E$, a reasonable value for active times [e.g. *Gorney et al.*, 1981]. At the same time, there is a five-fold increase in the number of ions reaching Geotail from the ionosphere. The increase in energy and outflow from the ionosphere are in good agreement with observations of increased ionospheric outflow and of an increase in the occurrence of ionospheric beams during active times [e.g. *Gorney et al.*, 1981; *Yau et al.*, 1985]. We note, however, that although the ionospheric distributions appear to be beam-like in nature, we cannot conclusively determine that beams are the only source of ionospheric outflow during this time, since we only measure the portion of the ionospheric outflow reaching the spacecraft.

Figure 7f shows that at 0840 UT more than two-thirds of the ions reaching Geotail are from the northern plasma mantle. These ions enter the magnetosphere from a broad region extending tailward from $x = -30\ R_E$. The number density of ions entering through this region shows two localized peaks in the near-Earth and far-tail regions (indicated by arrows in Figure 7f). Figure 13f shows that ions from the two regions have significantly different travel times to the spacecraft location. In order to investigate the existence of two seemingly distinct regions of entry at high latitudes, we examined the distribution of mantle ions and the configuration of the magnetosphere in detail.

Figures 16a and 16b show mantle distributions of the ions that entered the magnetosphere before and after 0800 UT, respectively. The distribution shown in Figure 16a was calculated between $x = -50\ R_E$ and $x = -60\ R_E$, while the distribution shown in Figure 16b was calculated for ions entering between $x = -80\ R_E$ and $x = -90\ R_E$. These locations were chosen to coincide with the two peaks in Figure 7f. The mantle distributions for the two locations are significantly different. Figure 16a shows a hot, accelerated, D-shaped distribution reminiscent of distributions found near reconnection regions [*Cowley*, 1984], with energies between 3 and 5 keV. Figure 16b, on the other hand, shows a cold, drifting population of the type traditionally associated with the plasma mantle [*Pilipp and Morfill*, 1978].

Since the substorm causes large-scale changes to the magnetospheric magnetic field topology, we would expect the high-latitude plasma mantle entry region to be affected. Recall that many of the ions from the Earthward mantle source observed at Geotail at 0840 UT had been in the magnetosphere for 2 hours or more (Figure 13f). We saw in Figure 6a that during the period of northward IMF (at t = 0700 UT), a high-latitude reconnection region existed. The hot mantle ions shown in Figure 16a were initially accelerated in this region. The D shape of the accelerated distribution is an established signature of reconnection [*Cowley*, 1984]. *Kessel et al.* [1996] investigated distributions measured onboard the Hawkeye satellite just earthward of a high-latitude reconnection region. While it is difficult to compare the 3D distributions calculated here (tailward of the reconnection region) with the 2D LEPEDEA distributions measured by *Kessel et al.*, they do show qualitative similarities between them, i.e. the accelerated D shape of

the distribution. Later, at 0800 UT (Figure 6b), dayside reconnection has already begun (at 0725 UT), and mantle ions enter on open field lines. As indicated earlier, these are ions traveling down an IMF field line that reconnects on the dayside and is swept downtail, resulting in an earthward-moving component in the plasma mantle population. This is the mantle source discussed by *Pilipp and Morfill* [1978]. Ions on these open field lines produce the cold source distribution shown in Figure 16b. This type of mantle entry occurs further downtail than the high-latitude reconnection entry region, resulting in the two distinct peaks seen in the entry plot shown in Figure 7f.

Having determined the entry and acceleration mechanisms responsible for mantle entry, we examine the trajectory of a typical ion from the high-latitude reconnection entry region to ascertain the role of this hot ion population in the plasma sheet. Figure 17 shows the trajectory of a typical ion from this region in a format similar to that of Figure 9. Early in its orbit, the particle bounces back and forth on freshly reconnected high-latitude field lines like those indicated by an arrow in Figure 6a. These changes in direction result from the presence of parallel electric fields along the magnetopause boundary, which cause the ion periodically to lose and gain energy during this part of its orbit (bottom panel of Figure 17, before ~ 0740 UT). These same fields eventually cause the ion to encounter a closed field line and reach Geotail ~ 2 hours after entering the magnetosphere. Thus, although the ions that enter through the reconnection region are much hotter than ions from any other source, they lose most of their energy before reaching closed field lines. In fact, the largest energy gain for these ions as well as those from the other plasma sources occurs because of non-adiabatic motion in the current sheet near the spacecraft (bottom panel of Figure 17).

5. Summary and Discussion

The vast regime of the magnetotail is sparsely covered by spacecraft, even in the ISTP era. In this paper, we have presented an effort that combines MHD modeling and LSK trajectory calculations in which the limited amount of data available at the Geotail spacecraft was used to

infer the source distributions of ions reaching the spacecraft during a magnetospheric substorm that occurred on November 24, 1996. Within the limitations of the MHD and LSK calculations, we present the following conclusions:

1. The Geotail spacecraft is positioned in the southern PSBL at the start of the interval examined. The rotation of the current sheet in response to the IMF and the changes associated with the onset of the expansion phase cause a gradual shift in the spacecraft's location, such that Geotail is found to be in the northern PSBL and lobe at the end of the interval examined.

2. Early in the growth phase, the Geotail ion distributions are dominated by ions from the LLBL. As the substorm progresses, contributions from the plasma mantle increase significantly. The reconfiguration of the magnetosphere during the expansion phase causes LLBL ions to lose access to the spacecraft location, and the mantle source (from both hemispheres) becomes dominant.

3. The ionosphere does not make a significant contribution to the Geotail distributions during this substorm, despite a five-fold increase in the number of ionospheric ions reaching Geotail between the growth and expansion phases of the substorm.

4. During the expansion phase, plasma mantle ions reaching Geotail do so by two different entry mechanisms. The first population enters in the near-Earth ($-30\ R_E < x < -50\ R_E$) mantle during a period of high-latitude reconnection preceding the substorm growth phase. Ions from this mantle source reach Geotail approximately two hours after entering the magnetosphere. The southward turning of the IMF at 0725 UT causes the reconnection region to shift to the dayside subsolar magnetopause. Mantle ions from the distant ($-70\ R_E < x < -100\ R_E$) mantle source enter on open field lines in the manner traditionally identified with the plasma mantle [*Pilipp and Morfill*, 1978] (as reported in *Ashour-Abdalla et al.*, 1999).

Observations of the magnetotail indicate that the quiet-time tail is populated predominantly by ions of solar wind origin, and that the number of ionospheric ions in the tail increases dramatically during active times [*Lennartsson and Shelley*, 1986, *Borovsky*, 1997]. Our analysis of the November 24, 1996 substorm indicates that the magnetotail plasma population near the Geotail location is dominated by solar wind ions; ionospheric ions increase in number fivefold during the expansion phase, but are still a small minority of the ion population. *Baker et al.* [1982] and later *Cladis and Francis* [1992] suggested that ionospheric ions, specifically O^+, are significant after substorm onset, especially during periods with multiple substorms. Because of

Geotail's motion into the northern lobes ~ 20 min into the expansion phase, we are unable to comment on this source later in the expansion phase; however, our results that the energy and the number of ionospheric ions increased early in the expansion phase are consistent with the ionosphere being a more important source late in the substorm. The relatively small number of ionospheric ions detected in this study can also be caused by the measurements having been made during the early phases of the substorm when the geopause occurred earthward of the spacecraft.

Perhaps the most important result obtained here is the calculation of distribution functions at the source regions supplying plasma to the magnetotail that can be compared with observations. Thus, starting from Geotail measurements in the near-Earth tail, we have used the tools of MHD and LSK to obtain information about the evolution of sources and about the evolution of the magnetospheric configuration during the time interval examined here. This is significant because, even in the ISTP era, there is a lack of satellite coverage in the magnetotail. The tool we have developed here allows us to take spacecraft observations and construct the history of the ion population in the magnetotail. We realize that the Geotail distributions allow us to construct only the portion of the source distribution reaching the spacecraft. However, a comparison of these source distributions with typical measured source distributions can give vital information on the entry and transport of plasma in the magnetotail.

Our analysis of this substorm has revealed many intriguing features that would have escaped detection were it not for the combination of techniques used here. Simulations and particle tracing techniques provide us with valuable tools for extracting the maximum amount of information from the observations available today.

Acknowledgments. We thank J. M. Bosqued and L. M. Zelenyi for many useful discussions. This work was supported by NASA grants NAG5-6689 and NAGW-4553 and the University of Iowa subcontract POV50494. Computing was provided by the UCLA Office of Academic Computing and by NPACI at the San Diego Supercomputer Center. UCLA-IGPP publication number 5254.

REFERENCES

Ashour-Abdalla, M., J. Berchem, J. Büchner, and L. M. Zelenyi, Shaping of the magnetotail from the mantle: Global and local structuring, *J. Geophys. Res.*, *98*, 5651, 1993.

Ashour-Abdalla, M., L. M. Zelenyi, V. Peroomian, and R. L. Richard, Consequences of magnetotail ion dynamics, *J. Geophys. Res.*, *99*, 14,891, 1994.

Ashour-Abdalla, M., L. M. Zelenyi, V. Peroomian, R. L. Richard, and J. M. Bosqued., The mosaic structure of plasma bulk flows in the Earth's magnetotail, *J. Geophys. Res.*, *100*, 19,191, 1995.

Ashour-Abdalla, et al., Ion sources and acceleration mechanisms inferred from local distribution functions *Geophys. Res. Lett.*, *24*, 955, 1997.

Ashour-Abdalla, M., J. Raeder, M. El Alaoui, V. Peroomian, magnetotail structure and its internal dynamics during northward IMF, in *New Perspectives on the Earth's Magnetotail*, edited by A. Nishida, D. N. Baker, and S. W. H. Cowley, *Geophys. Monogr. Ser.*, vol. 105, 77, AGU, Washington, D. C., 1998.

Ashour-Abdalla, M., M. El-Alaoui, V. Peroomian, R. J. Walker, J. Raeder, L. A. Frank, and W. R. Paterson, Source distributions of substorm ions observed in the near-Earth magnetotail, *Geophys. Res. Lett.*, *26*, 955, 1999.

Baker, D. N., E. W. Hones, Jr., D. T. Young, and J. Birn, The possible role of ionospheric oxygen in the initiation and development of plasma sheet instabilities, *Geophys. Res. Lett.*, *9*, 1337, 1982.

Berchem, J., J. Raeder, M. Ashour-Abdalla, L. A. Frank, W. R. Paterson, K. L. Ackerson, S. Kokubun, T. Yamamoto, R. P. Lepping, and K. Ogilvie, The distant tail at 200 R_E: Comparisons between Geotail observations and the result of global MHD simulations, *J. Geophys. Res.*, *103*, 9121, 1998*a*.

Berchem, J., J. Raeder, M. Ashour-Abdalla, L. A. Frank, W. R. Paterson, K. L. Ackerson, S. Kokubun, T. Yamamoto, and R. P. Lepping, Large-scale dynamics of the magnetospheric boundary: Comparisons between global MHD simulation results and ISTP observations, in *Geospace Mass and Energy Flow: Results From the International Solar-Terrestrial Physics Program*, edited by J. L. Horwitz, D. L. Gallagher, and W. K. Peterson, *Geophys. Monogr. Ser.*, vol. 104, 247, AGU, Washington, D. C., 1998*b*.

Borovsky, J. E., M. F. Thomsen, and D. J. McComas, The superdense plasma sheet: plasmaspheric origin, solar wind origin, or ionospheric origin?, *J. Geophys. Res.*, *97*, 22,089, 1997.

Büchner, J., and L. M. Zelenyi, Deterministic chaos in the dynamics of charged particles near a magnetic field reversal, Phys. Lett. A, 118, 395, 1986.

Büchner, J. and L. Zelenyi, Regular and chaotic charged particle motion in magnetotail-like field reversals. 1. Basic theory of trapped motion, *J. Geophys. Res.*, *94*, 11,821, 1989.

Chappel, C. R., R. E. Moore, and J. H. Waite, Jr., The ionosphere as a fully adequate source of plasma for the Earth's magnetosphere, *J. Geophys. Res.*, *92*, 5896, 1987.

Chen, J., and P. J. Palmadesso, Chaos and nonlinear dynamics of single-particle orbits in a magnetotaillike magnetic field, J. Geophys. Res., 91, 1499, 1986.

Cladis, J. B., and W. E. Francis, The polar ionosphere as a source of the storm time ring current, J. Geophys. Res., 90, 3465, 1985.

Cladis, J. B. and W. E. Francis, Distribution in magnetotail of O^+ ions from cusp/cleft ionosphere: a possible substorm trigger, *J. Geophys. Res.*, *97*, 123, 1992.

Cowley, S. W. H., Plasma populations in a simple open model magnetosphere, *Space Sci. Rev.*, *26*, 217, 1980.

Cowley, S. W. H., The distant geomagnetic tail in theory and observation, in *Magnetic Reconnection in Space and Laboratory Plasmas*, edited by E. W. Hones, Jr., *Geophys. Monogr. Ser.*, *30*, 228, AGU, Washington, D. C., 1984.

Delcourt, D. C., C. R. Chappell, T. E. Moore, and J. H. Waite, Jr., A three-dimensional numerical model of ionospheric plasma in the magnetosphere, *J. Geophys. Res.*, *94*, 11,893, 1989.

Delcourt, D. C., J. A. Sauvaud, and T. E. Moore, Cleft Contribution to Ring Current Formation, *J. Geophys. Res.*, *95*, 20937, 1990.

Delcourt, D. C., J. A. Sauvaud, R. F. Martin, Jr., and T. E. Moore, Gyrophase effects in the centrifugal impulse model of particle motion in the magnetotail, , *J. Geophys. Res.*, *100*, 17,211, 1995.

Eastman, T.E., E.W. Hones, Jr., S.J. Bame, and J. R. Asbridge, The magnetospheric boundary layer: Site of plasma, momentum and energy transfer from the magnetosheath to the magnetosphere, *Geophys. Res. Lett.*, *3*, 685, 1976.

Eastman, T. E., and E. W. Hones, Jr., Characteristics of the magnetospheric boundary layer and magnetopause layer as observed by Imp 6, *J. Geophys. Res.*, *84*, 2019, 1979.

El-Alaoui, M., Current disruption during the November 24, 1996 substorm, *J. Geophys. Res.*, submitted, 1999.

Frank, L. A et al., The Comprehensive Plasma Instrumentation (CPI) for the Geotail spacecraft, *J. Geomag. Geoelec.*, *46*, 23, 1994.

Frank, L. A., M. Ashour-Abdalla, J. Berchem, J. Raeder, W. R. Paterson, S. Kokubun, T. Yamamoto, R. P. Lepping, F. V. Coroniti, D. H. Fairfield, and K. L. Ackerson, Observations of plasmas and magnetic field in Earth's distant magnetotail: Comparison with a global MHD model, *J. Geophys. Res.*, *100*, 19,177, 1995.

Goodrich, C. C., J. G. Lyon, M. Wiltberger, R. E. Lopez, and K. Papadopoulos, An overview of the impact of the January 10-11, 1997 magnetic cloud on the magnetosphere via global MHD simulation, *Geophys. Res. Lett.*, *25*, 2537, 1998.

Gorney, D. J., A. Clarke, D. Croley, J. F. Fennell, J. Luhmann, and P. Mizera, The Distribution of ion Beams and Conics Below 8000 km, J. Geophys. Res., 86, 83, 1981.

Hamilton, D. C., G. Gloeckler, F. M. Ipavich, W. Stüdemann, B. Wilken, and G. Kremser, Ring Current Development During the Great Geomagnetic Storm of February 1986, *J. Geophys. Res.*, *93*, 14343, 1988.

Kessel, R. L., et al., Evidence of high-latitude reconnection during northward IMF: Hawkeye observations, *Geophys. Res. Lett.*, *23*, 583, 1996.

Kokubun, S., T. Yamamoto, M. H. Acuña, K. Hayashi, K. Shiokawa, and H. Kawano, The Geotail magnetic field experiment, *J. Geomag. Geoelec.*, *46*, 7, 1994.

Knight, S., Parallel electric fields, *Planet. Space Sci.*, *21*, 741, 1972.

Lennartsson, W. and E. G. Shelley, Survey of 0.1- to 16-keV/e plasma sheet ion compositions, *J. Geophys. Res.*, *91*, 3061, 1986.

Lennartsson, W., A scenario for solar wind penetration of Earth's magnetic tail based on ion composition data from the ISEE 1 spacecraft, *J. Geophys. Res.*, *97*, 19,221, 1992.

Lockwood, M., J. H. Waite Jr., T. E. Moore, J. F. E. Johnson, and C. R. Chappell, A new source of suprathermal O^+ ions near the dayside polar cap boundary, J. Geophys. Res., 90, 4099, 1985a.

Lockwood, M., M. O. Chandler, J. L. Horwitz, J. H. Waite, Jr., T. E. Moore, and C. R. Chappell, The cleft ion fountain, J. Geophys. Res., 90, 9376, 1985b.

Lyons, L. R., D. Evans, and R. Lundin, An observed relation between magnetic field aligned electric fields and downward electron energy fluxes in the vicinity of auroral forms, *J. Geophys. Res.*, *84*, 457, 1979.

Lyons, L. R., and T. W. Speiser, Evidence for current sheet acceleration in the geomagnetic tail, *J. Geophys. Res.*, *87*, 2276, 1982.

Mauk, B. H., Quantitative modeling of the "convective surge" mechanism of ion acceleration, J. Geophys. Res., 91, 13,423, 1986.

Mitchell, D. G., F. Kutchko, D. J. Williams, T. E. Eastman, L. A. Frank, and C. T. Russell, An extended study of the low-latitude boundary layer on the dawn and dusk flanks of the magnetosphere, *J. Geophys. Res.*, *92*, 7394, 1987.

Moen, J., and A. Brekke, The solar flux influence on quiet time conductances in the auroral ionosphere, *Geophys. Res. Lett.*, *20*, 971, 1993.

Moore, T. E., Origins of magnetospheric plasma, U. S. Natl. Rep. Int. Union Geod. Geophys. 1987-1990, *Rev. Geophys.*, *29*, 1039, 1991.

Moore, T. E., and D. C. Delcourt, The Geopause, *Rev. Geophys.*, *33*, 175, 1995.

Peroomian, V., and M. Ashour-Abdalla, Relative contribution of the solar wind and the auroral zone to near-Earth plasmas, in *Cross-Scale Coupling in Space Plasmas*, edited by J. Horwitz et al., *Geophys. Monogr. Ser.*, vol. 93, , pp. 213-217, AGU, Washington, D. C., 1995.

Peroomian, V., and M. Ashour-Abdalla, Population of the near-Earth magnetotail from the auroral zone, *J. Geophys. Res.*, *101*, 15,387, 1996.

Pilipp, W. G., and G. Morfill, The formation of the plasma sheet resulting from plasma mantle dynamics, J. Geophys. Res., 83, 5670, 1978.

Raeder, J., R. J. Walker, and M. Ashour-Abdalla, The structure of the distant geomagnetic tail during long periods of northward IMF, *Geophys. Res. Lett.*, *22*, 349, 1995.

Raeder, J., J. Berchem, and M. Ashour-Abdalla, The importance of small-scale processes in global MHD simulations: Some numerical experiments, in *The Physics of Space Plasmas*, vol. 14, T. Chang and J. R. Jasperse, eds., p. 403, MIT Center for Theoretical Geo/Cosmo Plasma Physics, Cambridge, MA. 1996.

Raeder, J., J. Berchem, M. Ashour-Abdalla, L. A. Frank, W. R. Paterson, K. L. Ackerson, J. M. Bosqued, R. P. Lepping, S. Kokubun, T. Yamamoto, S. A. Slavin, Boundary layer formation in the magnetotail: Geotail observations and comparisons with a global MHD model, *Geophys. Res. Lett.*, *24*, 951, 1997.

Robinson, R. M., R. R. Vondrak, K. Miller, T. Dabbs, and D. Hardy, On calculating ionospheric conductances from the flux and energy of precipitating electrons, *J. Geophys. Res.*, *92*, 2565, 1987.

Sergeev, V. A., and B. B. Gvozdevsky, MT-index – a possible new index to characterize the magnetic configuration of the magnetotail, *Ann. Geophys.*, *13*, 1093, 1995.

Shelley, E. G., R. G. Johnson, and R. D. Sharp, Satellite Observations of Energetic Heavy Ions during a Geomagnetic Storm, *J. Geophys. Res.*, *77*, 6104, 1972.

Song, P. and C. T. Russell, Model of the formation of the low-latitude boundary layer for strongly northward interplanetary magnetic field, *J. Geophys. Res.*, *97*, 1411, 1992.

Speiser, T. W., Particle trajectories in model current sheets, J. Geophys. Res., 70, 4219, 1965.

Winglee, R. M., Multi-fluid simulations of the magnetosphere: the identification of the geopause and its variation with IMF, *Geophys. Res. Lett.*, *25*, 4441, 1998.

Yau, A. W., E. G. Shelley, W. K. Peterson, and L. Lenchyshyn, Energetic auroral and polar ion outflow at DE 1 altitudes: magnitude, composition, magnetic activity dependence, and long-term variations, *J. Geophys. Res.*, *90*, 8417, 1985.

Table 1.

Time (UT)	Geotail Location	Substorm Phase	% Nonadiabatic
0740	Southern PSBL	Growth	25
0750	Plasma Sheet	Growth	43
0800	Plasma Sheet	Growth	35
0810	Plasma Sheet	Growth	42
0830	Outer CPS	Expansion	3
0840	Northern PSBL	Expansion	14

Figure Captions

Figure 1. CANOPUS magnetometer data for November 24, 1996.

Figure 2. WIND data for November 24, 1996.

Figure 3. V_Y-V_Z, V_X-V_Z, and V_X-V_Y cuts of the Geotail distribution for six time intervals. Peak fluxes in the central parts of the distributions correspond to 2×10^{-24} s^3/cm^{-6}. The distributions are cut off at a flux level of 2×10^{-26} s^3/cm^{-6}.

Figure 4. Geotail measurements in the magnetotail, showing profiles of (a) B_X, (b) B_Y, (c) B_Z, and (d) V_X.

Figure 5. MHD pressure profiles in the x - z (left-hand column) and y - z (right-hand column) planes intersecting the Geotail location at (a,d) 0800 UT, (b,e) 0830 UT, and (c,f) 0902 UT.

Figure 6. Field lines from MHD model for (a) 0700 UT (northward IMF) arrow indicates high-latitude reconnection region, (b) 0800 UT (southward IMF).

Figure 7. Magnetotail entry points for the ions in the Geotail distribution functions observed at (a) 0740 UT, (b) 0750 UT, (c) 0800 UT, (d) 0810 UT, (e) 0830 UT, and (f) 0840 UT. Field line color coding is: red – closed, white – open, magenta – IMF.

Figure 8. Percentage of ions measured by Geotail as a function of time that originate from the northern and southern plasma mantle (solid curve), the LLBL (dotted curve) and the ionosphere (dashed curve).

Figure 9. Trajectory of a duskside LLBL particle reaching Geotail at 0740 UT projected onto the (top panel) $x-z$ and (middle panel) $x-y$ planes. (Lower Panel) Kinetic energy (black curve, scale on left) and κ (gray dots, scale on right) for the particle.

Figure 10. Trajectory of a northern plasma mantle particle reaching Geotail at 0840 UT in a similar format to that of Fig. 7.

Figure 11. Trajectory of an ionospheric particle reaching Geotail at 0840 UT in a similar format to that of Fig. 7.

Figure 12. Magnetotail entry points for ions reaching Geotail at (a) 0800 UT and (b) 0840 UT. The color coding corresponds to the percentage of non-adiabatic ($\kappa < 2$) ions in each 1 R_E^3 bin.

Figure 13. Projection of magnetotail entry points onto the $x-z$ plane for the six time intervals. Color coding indicates the time of flight between the source and the point of measurement.

Figure 14. $V_x - V_z$ Distribution of LLBL ions that reach Geotail at (a) 0740 UT, (b) 0800 UT, and (c) 0830 UT.

Figure 15. $V_{\|} - V_{\perp}$ distribution functions measured at ionosphere for particles reaching Geotail at (a) 0740 UT and (b) 0840 UT.

Figure 16. $V_x - V_z$ Distribution of mantle ions that reach Geotail at 0840 UT. (a) ions entering before 0800 UT, and (b) ions entering after 0800 UT.

Figure 17. Trajectory of an ion entering through the high latitude reconnection region and reaching Geotail at 0840 UT, in a similar format to that of Fig. 7.

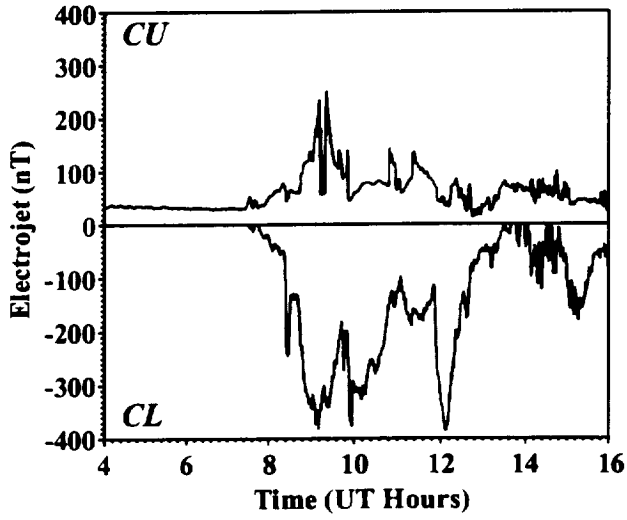
CU
CL
400
300
200
100
0
-100
-200
-300
-400
Electrojet (nT)
4
6
8
10
12
14
16
Time (UT Hours)

Figure 1

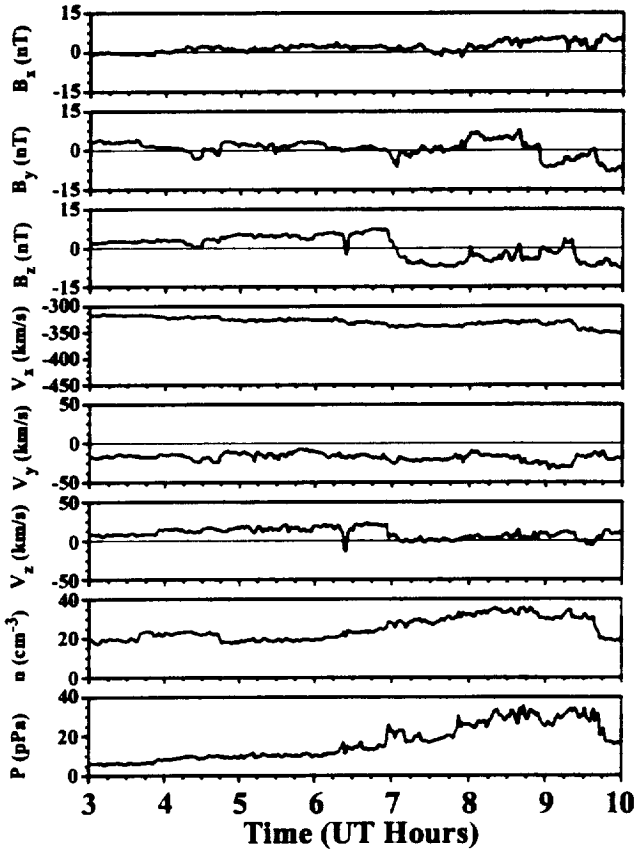
15
0
-15
B_x (nT)
15
0
-15
B_y (nT)
15
0
-15
B_z (nT)
-300
-350
-400
-450
V_x (km/s)
50
0
-50
V_y (km/s)
50
0
-50
V_z (km/s)
40
20
0
n (cm^{-3})
40
20
0
P (pPa)
3
4
5
6
7
8
9
10
Time (UT Hours)

Figure 2

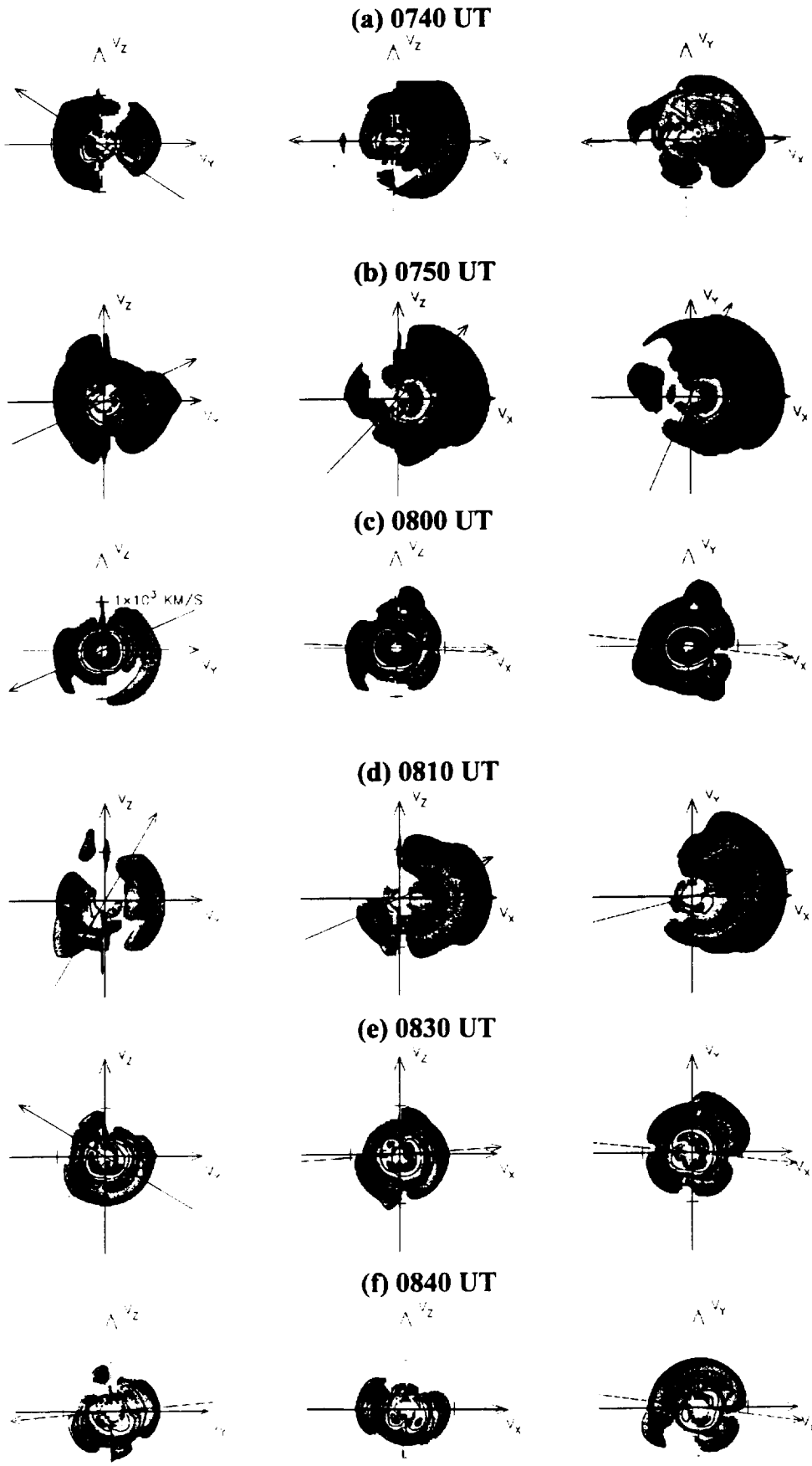
(a) 0740 UT
(b) 0750 UT
(c) 0800 UT
1x10³ KM/S
(d) 0810 UT
(e) 0830 UT
(f) 0840 UT

Figure 3

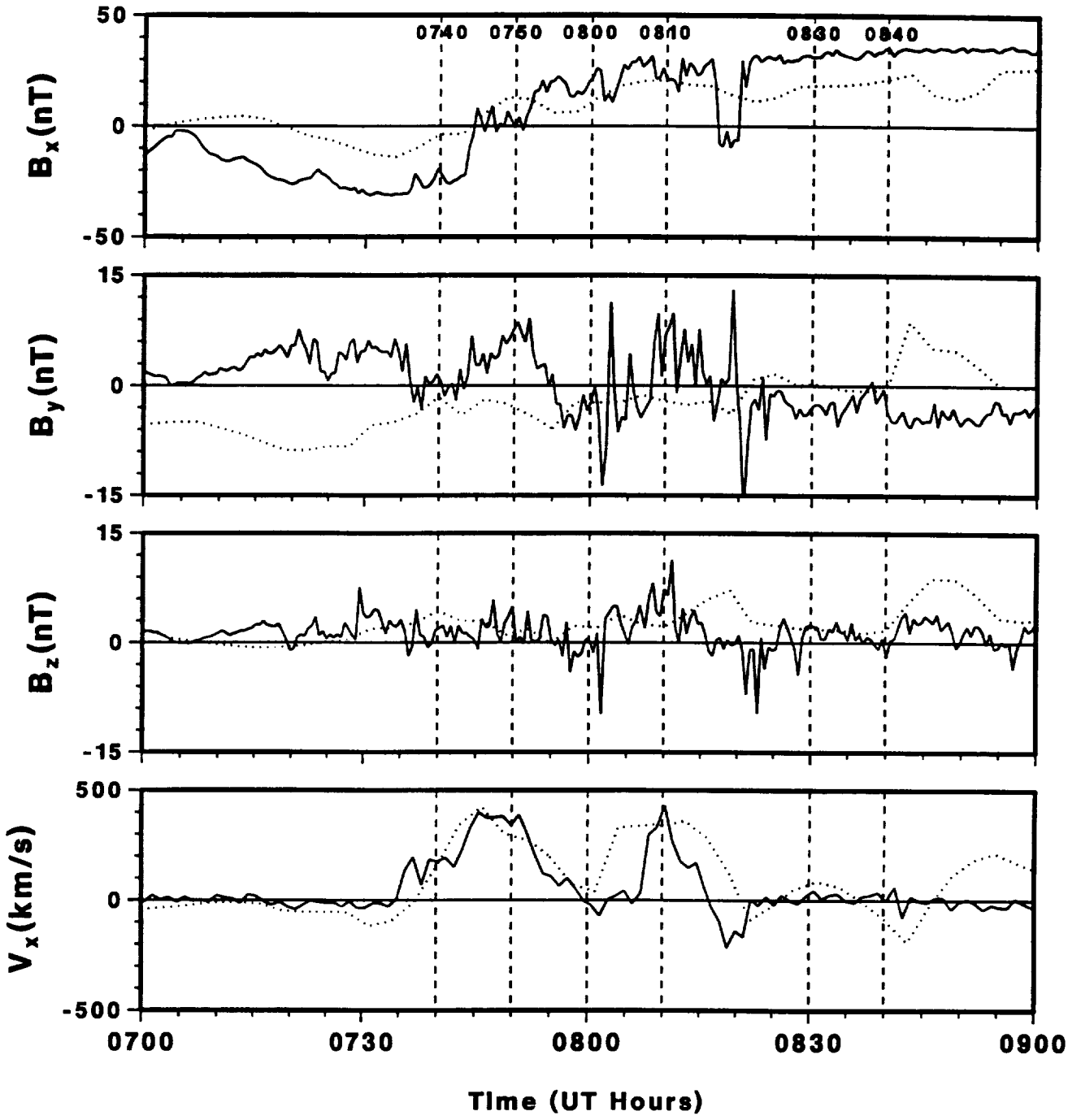
50
0
-50
B_x(nT)
0740
0750
0800
0810
0830
0840
15
0
-15
B_y(nT)
15
0
-15
B_z(nT)
500
0
-500
V_x(km/s)
0700
0730
0800
0830
0900
Time (UT Hours)

Figure 4

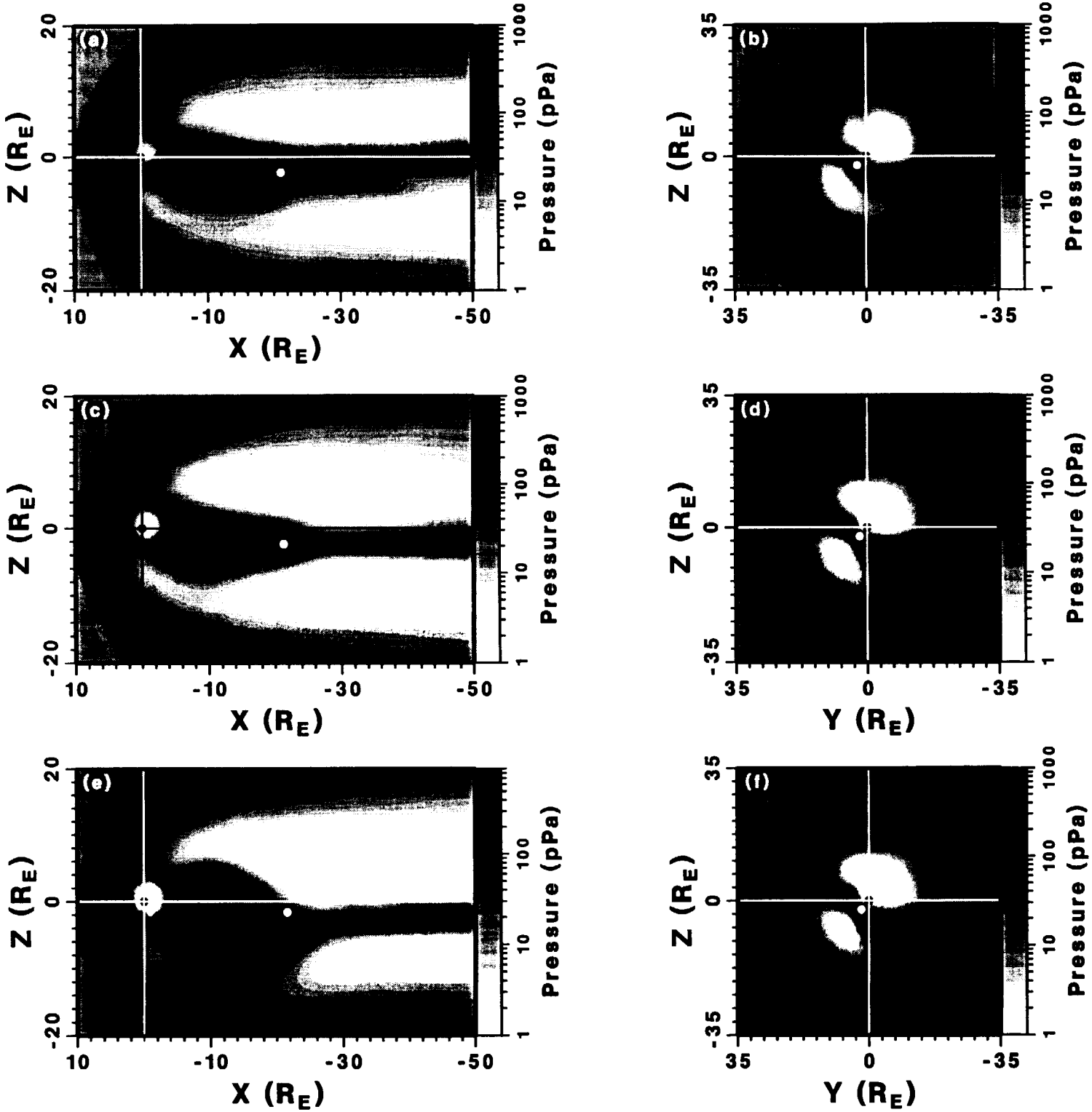
(a)
(b)
(c)
(d)
(e)
(f)
Z (R_E)
X (R_E)
Y (R_E)
Pressure (pPa)
20
0
-20
10
-10
-30
-50
35
-35
1000
100
10
1

Figure 5

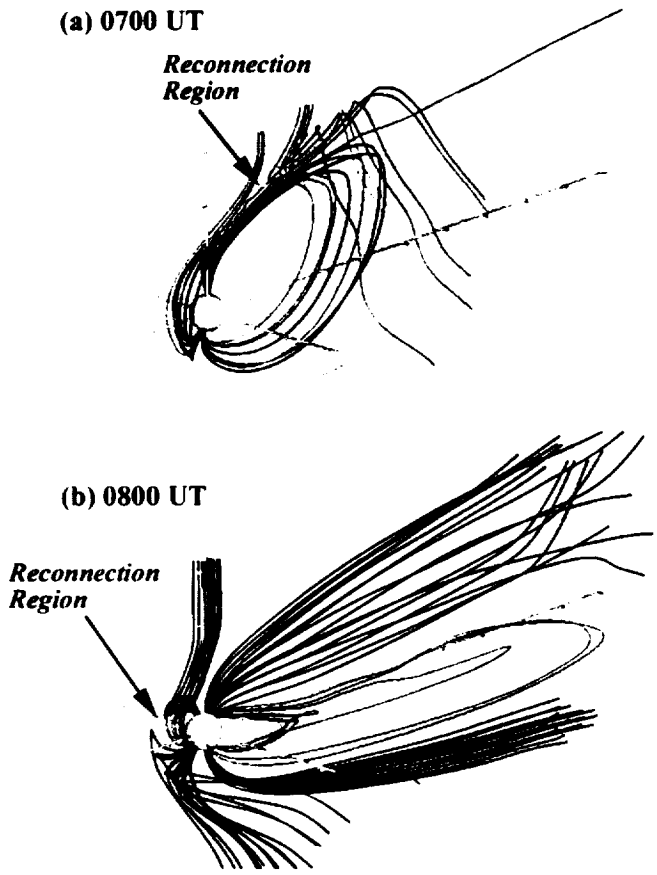
(a) 0700 UT
Reconnection Region
(b) 0800 UT
Reconnection Region

Figure 6

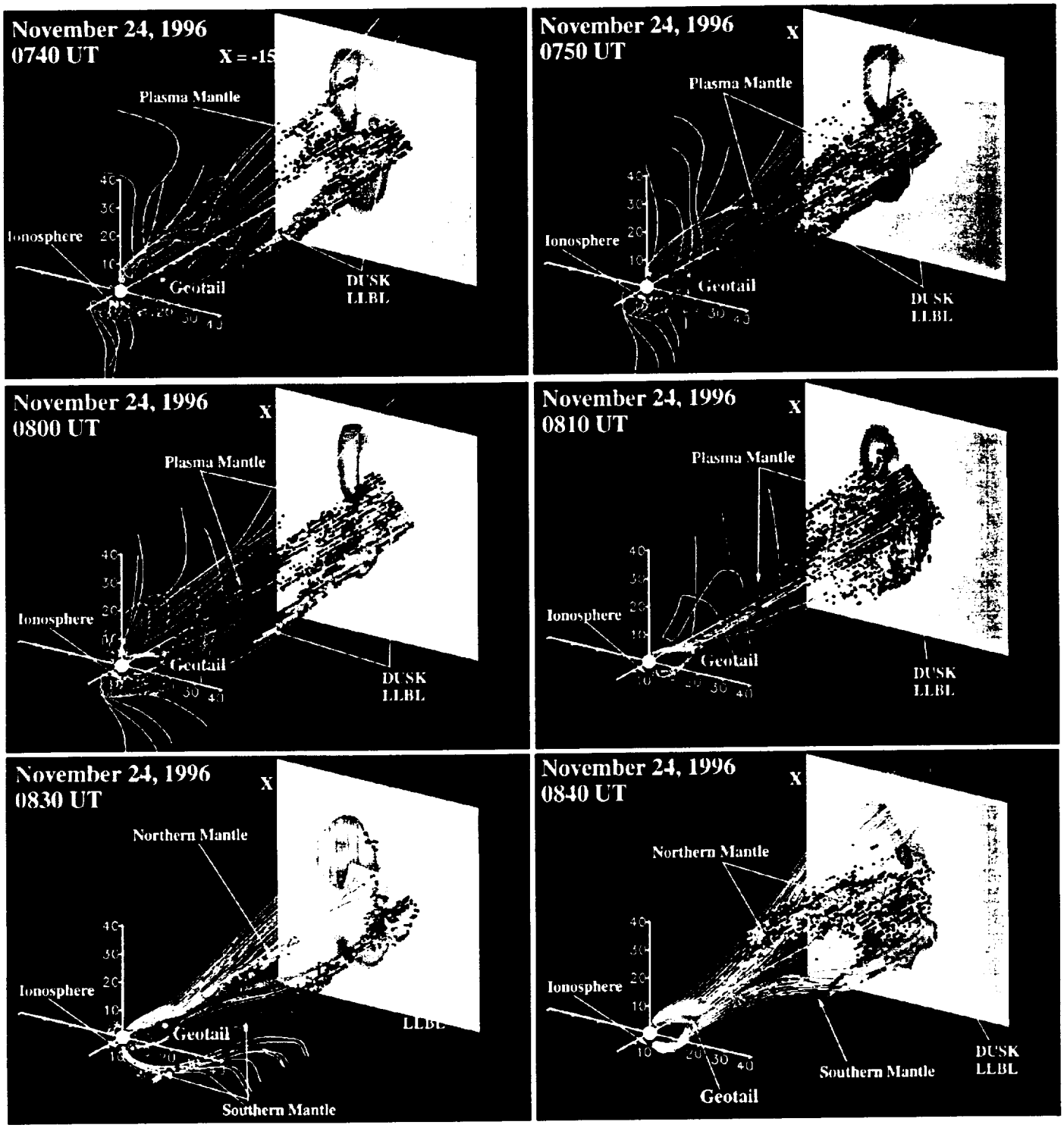
November 24, 1996
0740 UT
X = -15
Plasma Mantle
Ionosphere
Geotail
DUSK
LLBL
November 24, 1996
0750 UT
X
Plasma Mantle
Ionosphere
Geotail
DUSK
LLBL
November 24, 1996
0800 UT
X
Plasma Mantle
Ionosphere
Geotail
DUSK
LLBL
November 24, 1996
0810 UT
X
Plasma Mantle
Ionosphere
Geotail
DUSK
LLBL
November 24, 1996
0830 UT
X
Northern Mantle
Ionosphere
Geotail
Southern Mantle
November 24, 1996
0840 UT
X
Northern Mantle
Ionosphere
Southern Mantle
DUSK
LLBL
Geotail

Figure 7

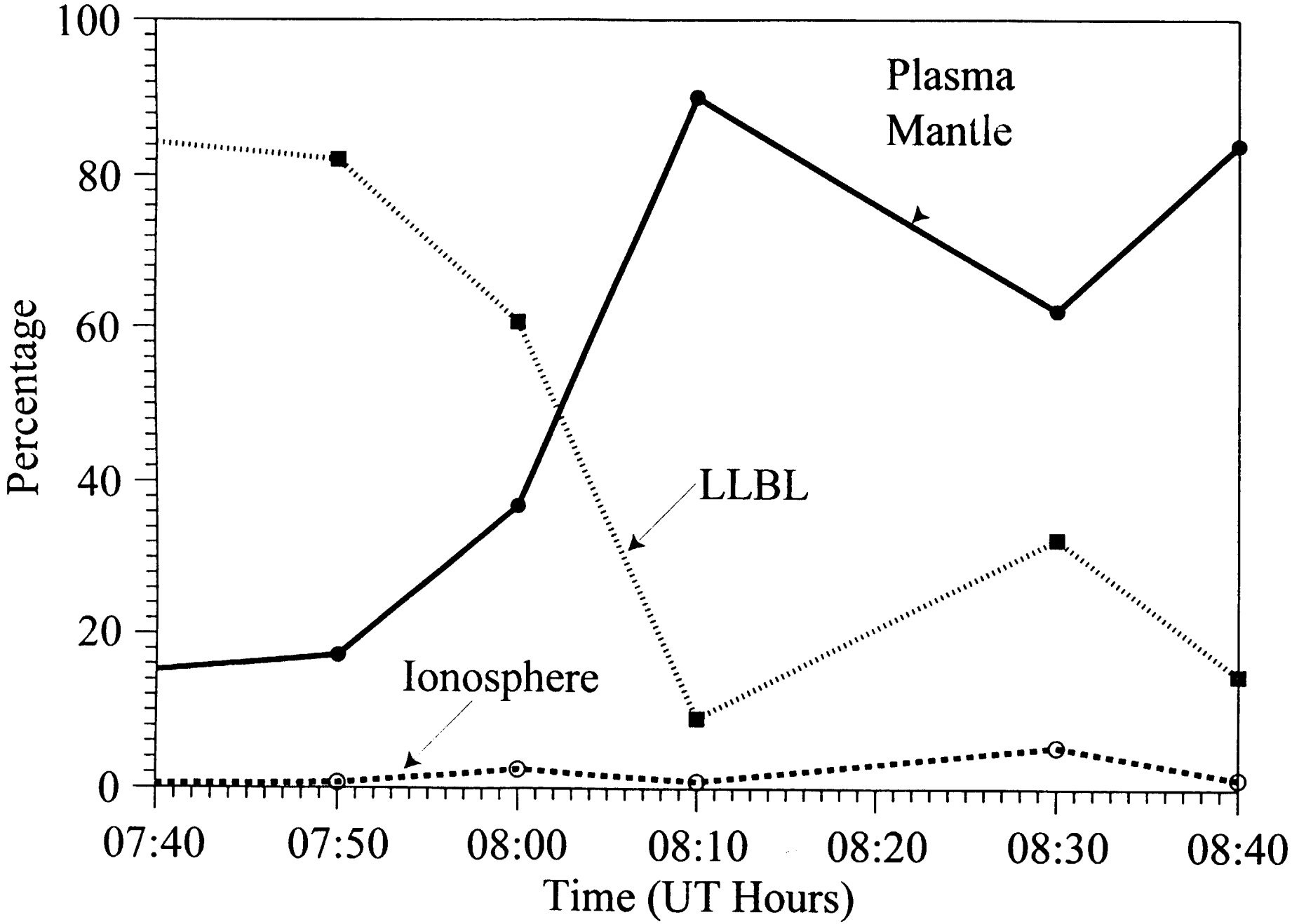
100
80
60
40
20
0
Percentage
Plasma
Mantle
LLBL
Ionosphere
07:40
07:50
08:00
08:10
08:20
08:30
08:40
Time (UT Hours)

Figure 8

Duskside LLBL Ion

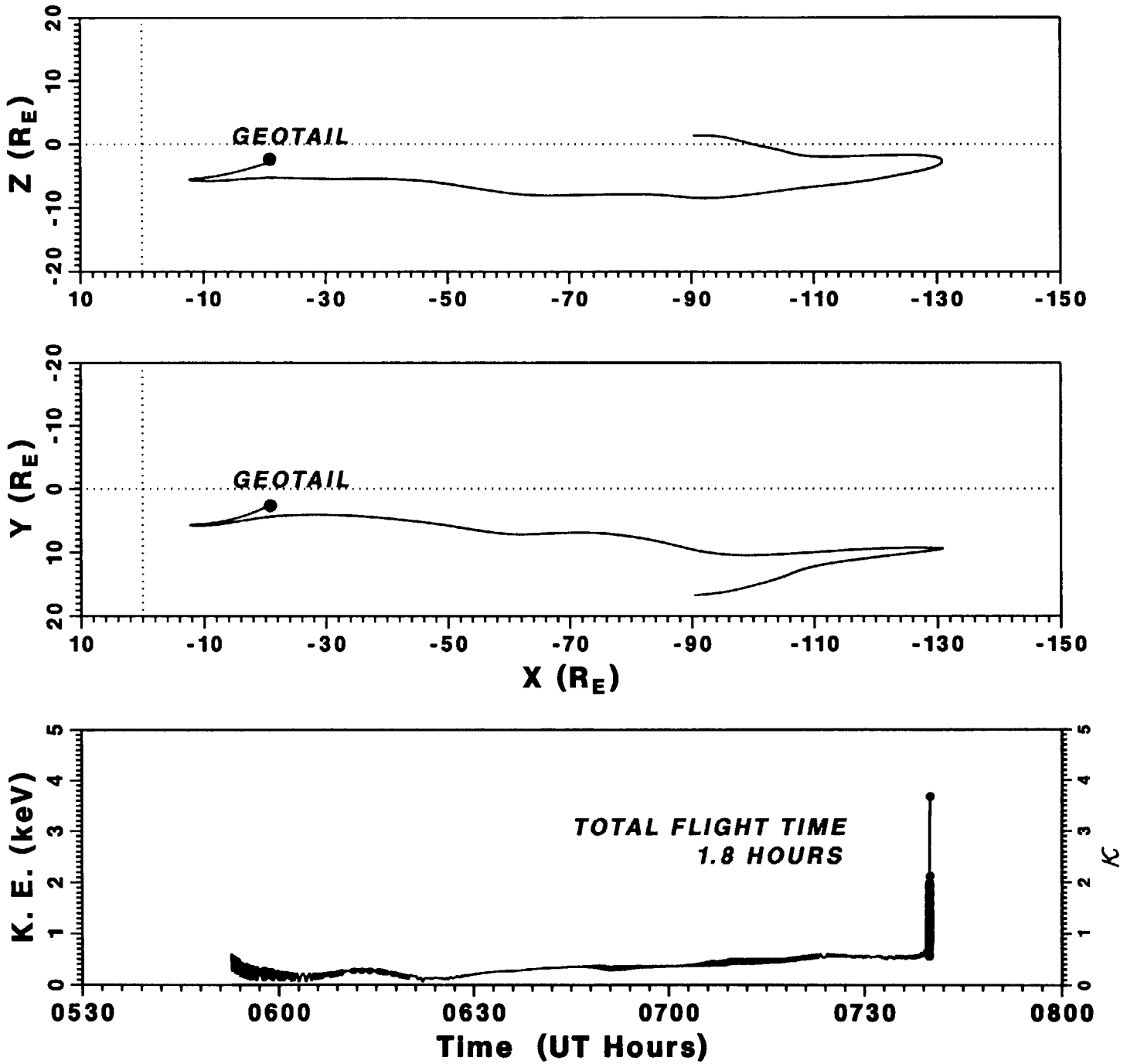

Figure 9

Plasma Mantle Ion

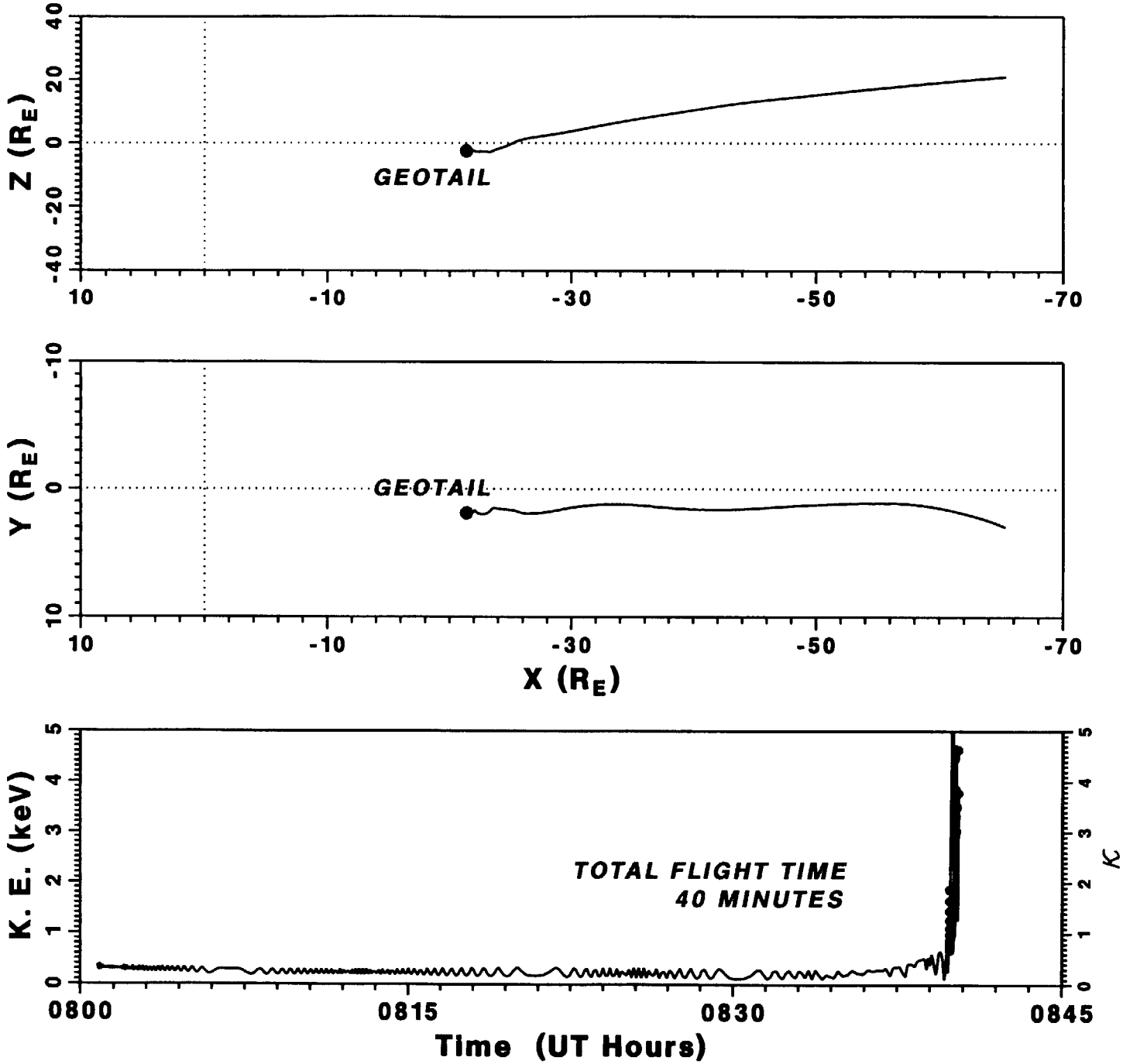

Figure 10

Accelerated Ionospheric Ion

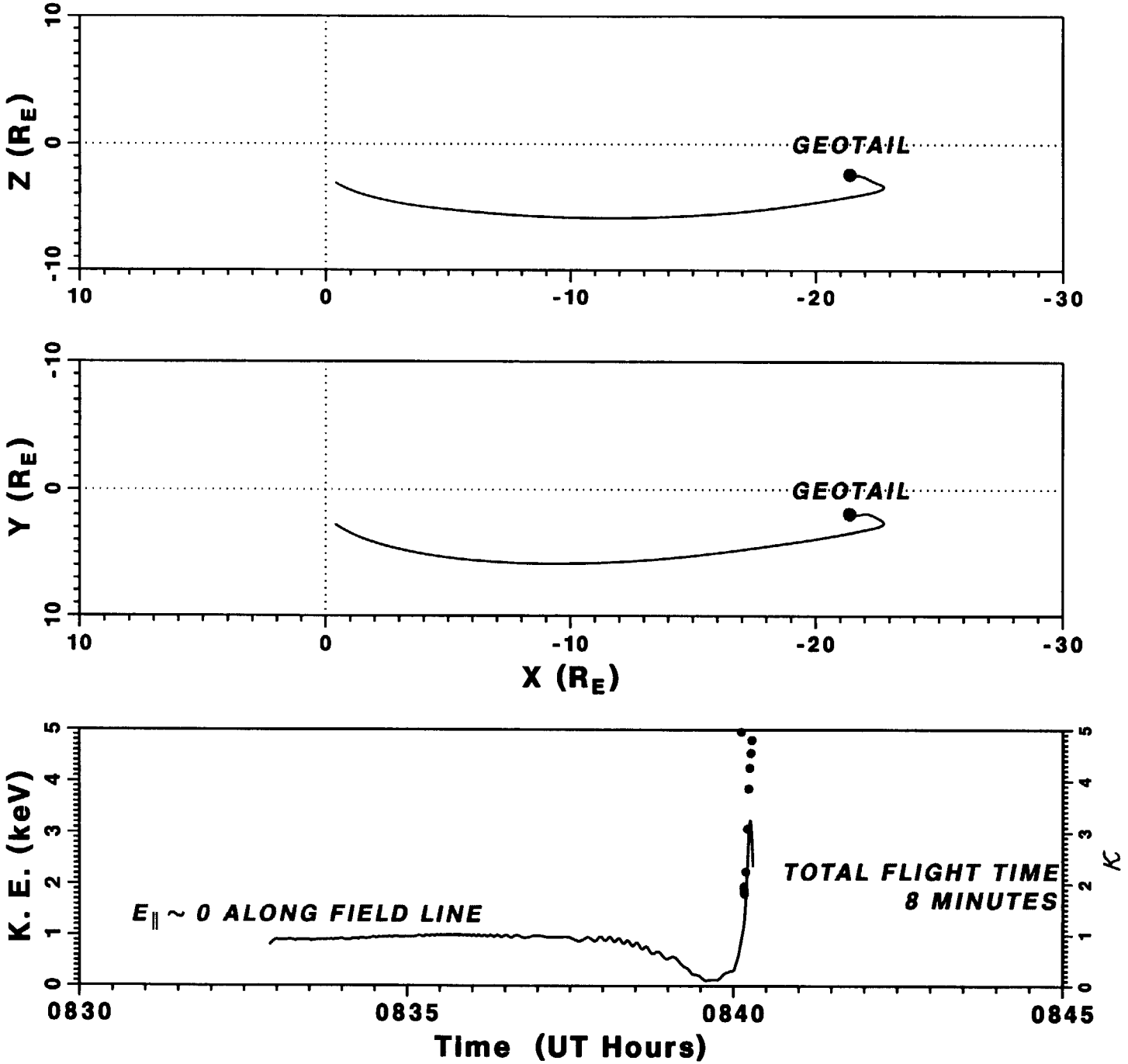

Figure 11

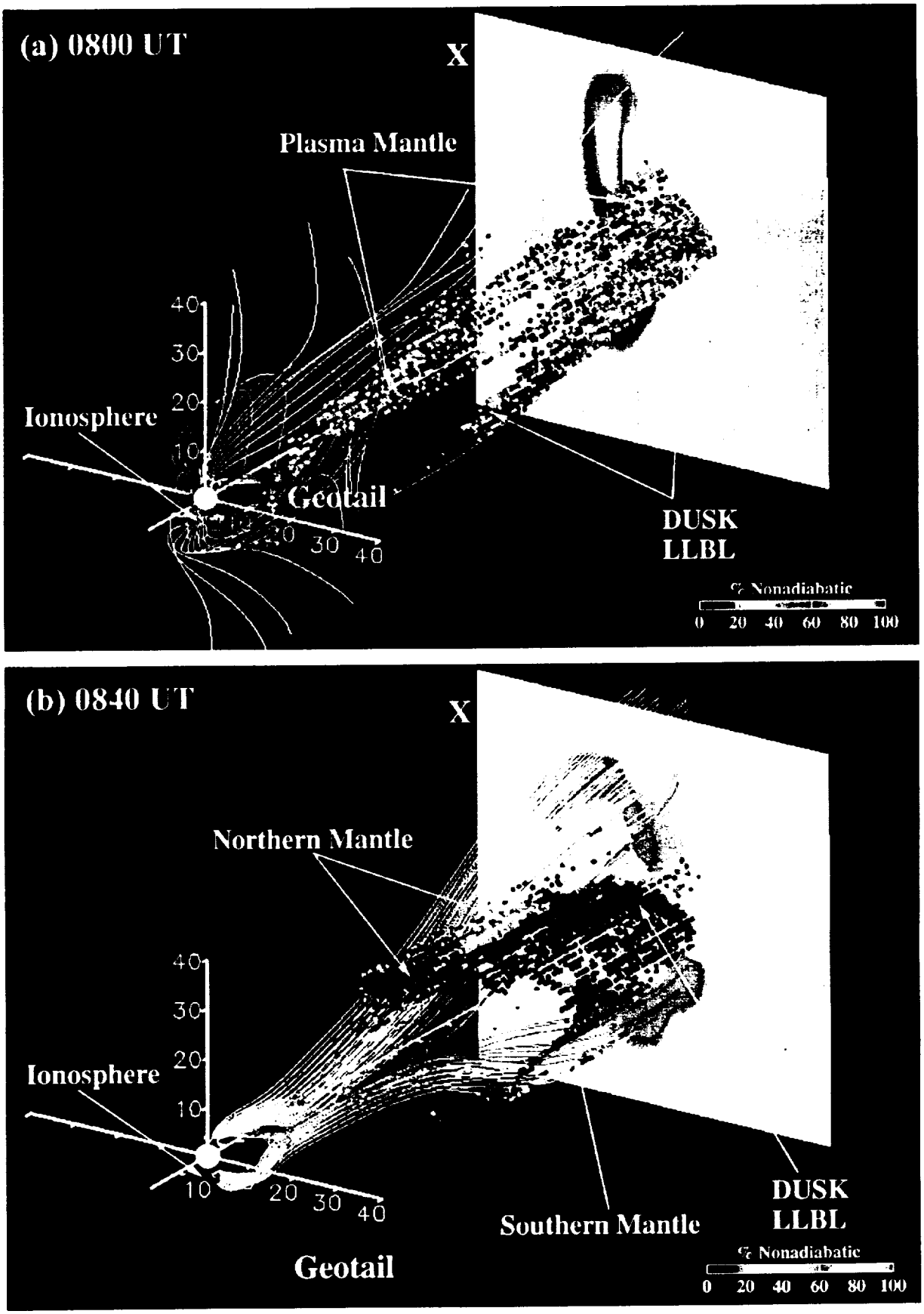
(a) 0800 UT
X
Plasma Mantle
Ionosphere
Geotail
DUSK
LLBL
% Nonadiabatic
0 20 40 60 80 100
(b) 0840 UT
X
Northern Mantle
Ionosphere
Geotail
Southern Mantle
DUSK
LLBL
% Nonadiabatic
0 20 40 60 80 100

Figure 12

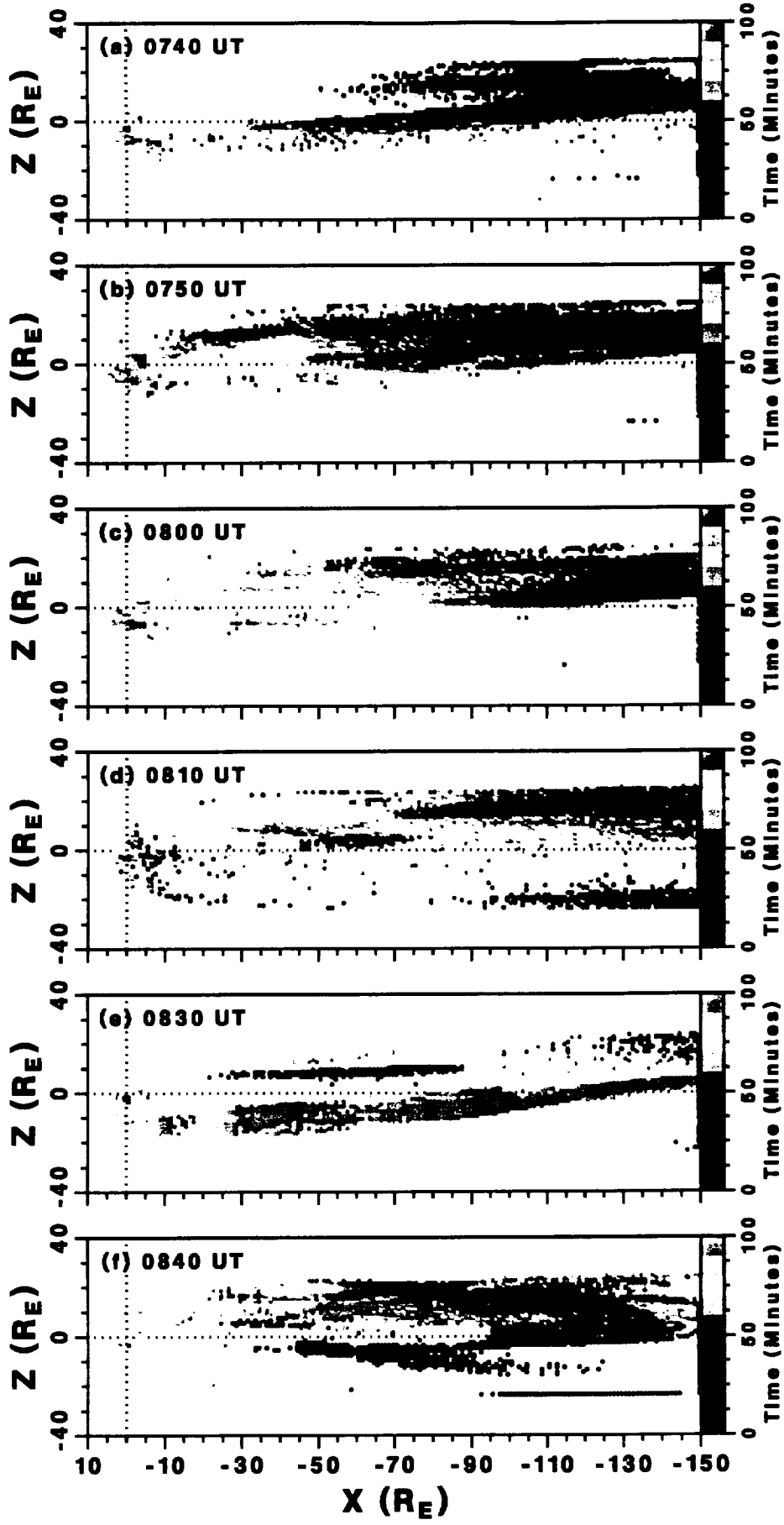
(a) 0740 UT
(b) 0750 UT
(c) 0800 UT
(d) 0810 UT
(e) 0830 UT
(f) 0840 UT
Z (R_E)
40
0
-40
Time (Minutes)
100
50
0
10
-10
-30
-50
-70
-90
-110
-130
-150
X (R_E)

Figure 13

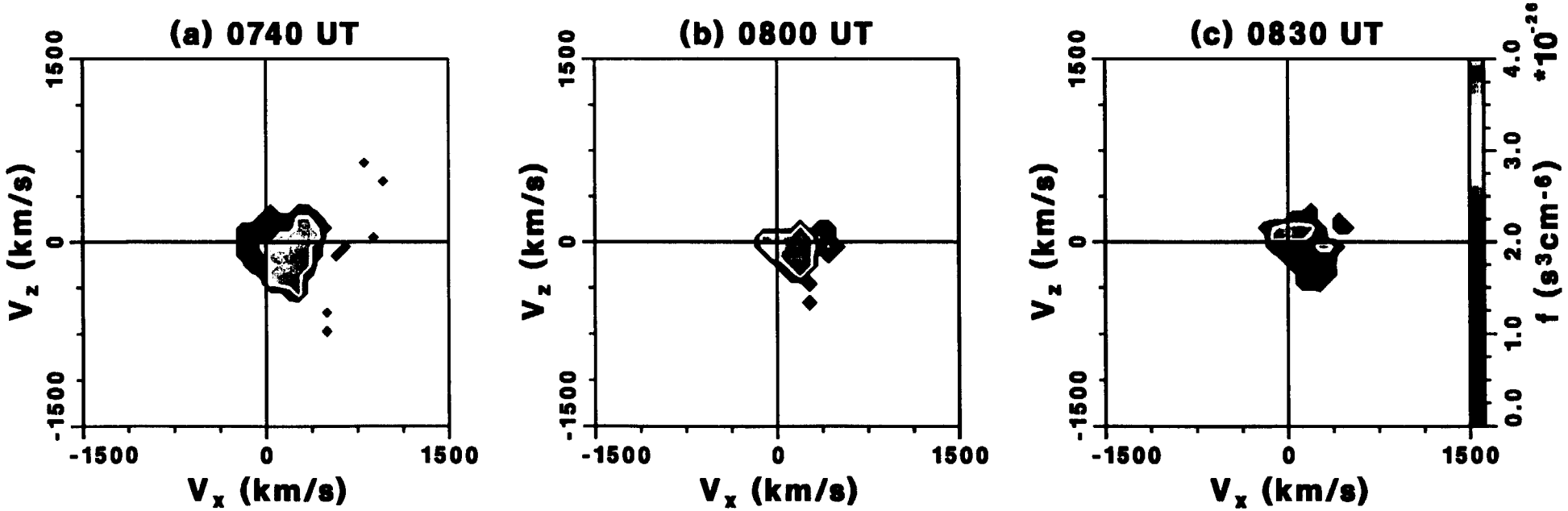
(a) 0740 UT
(b) 0800 UT
(c) 0830 UT
V_z (km/s)
V_x (km/s)
1500
0
-1500
f (s^3cm^-6)
*10^-26
4.0
3.0
2.0
1.0
0.0

Figure 14

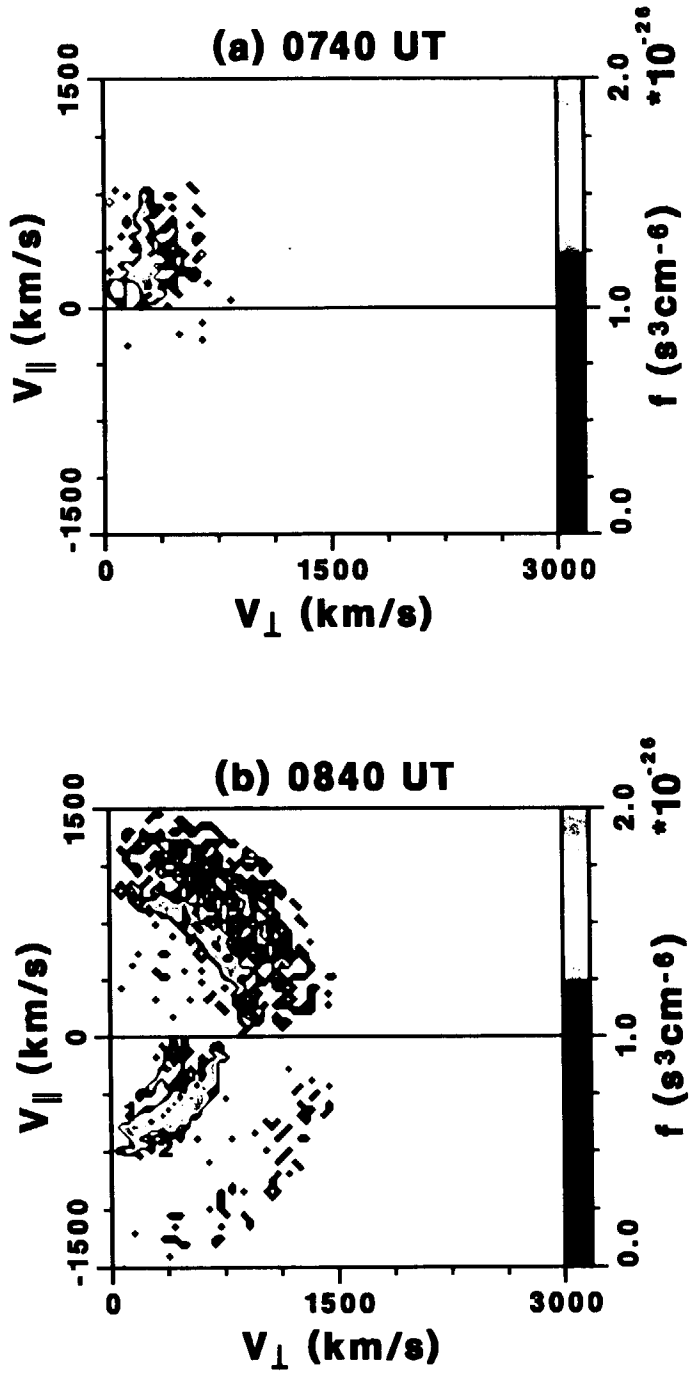
(a) 0740 UT
(b) 0840 UT
1500
0
-1500
0
1500
3000
$V_\perp$ (km/s)
$V_\parallel$ (km/s)
2.0
1.0
0.0
*10^{-26}
f (s^{3}cm^{-6})

Figure 15

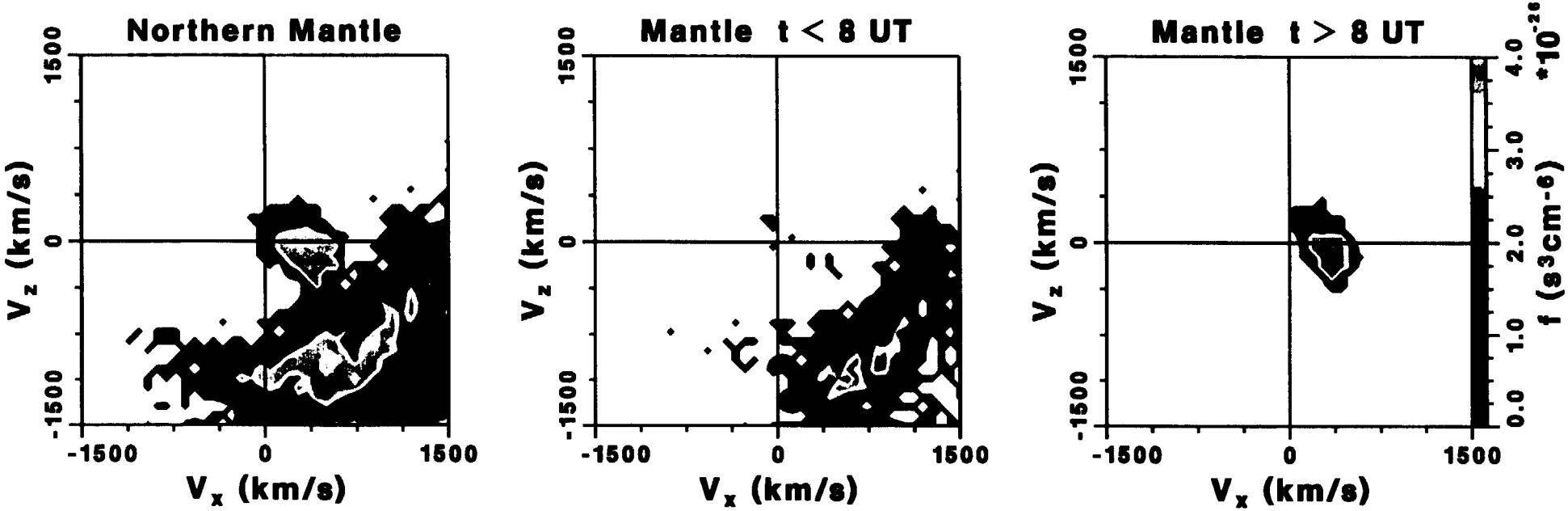
Northern Mantle
Mantle t < 8 UT
Mantle t > 8 UT
V_z (km/s)
V_x (km/s)
1500
0
-1500
f (s^3cm^-6)
*10^-26
0.0
1.0
2.0
3.0
4.0

Figure 16

Plasma Mantle Ion From Reconnection Region

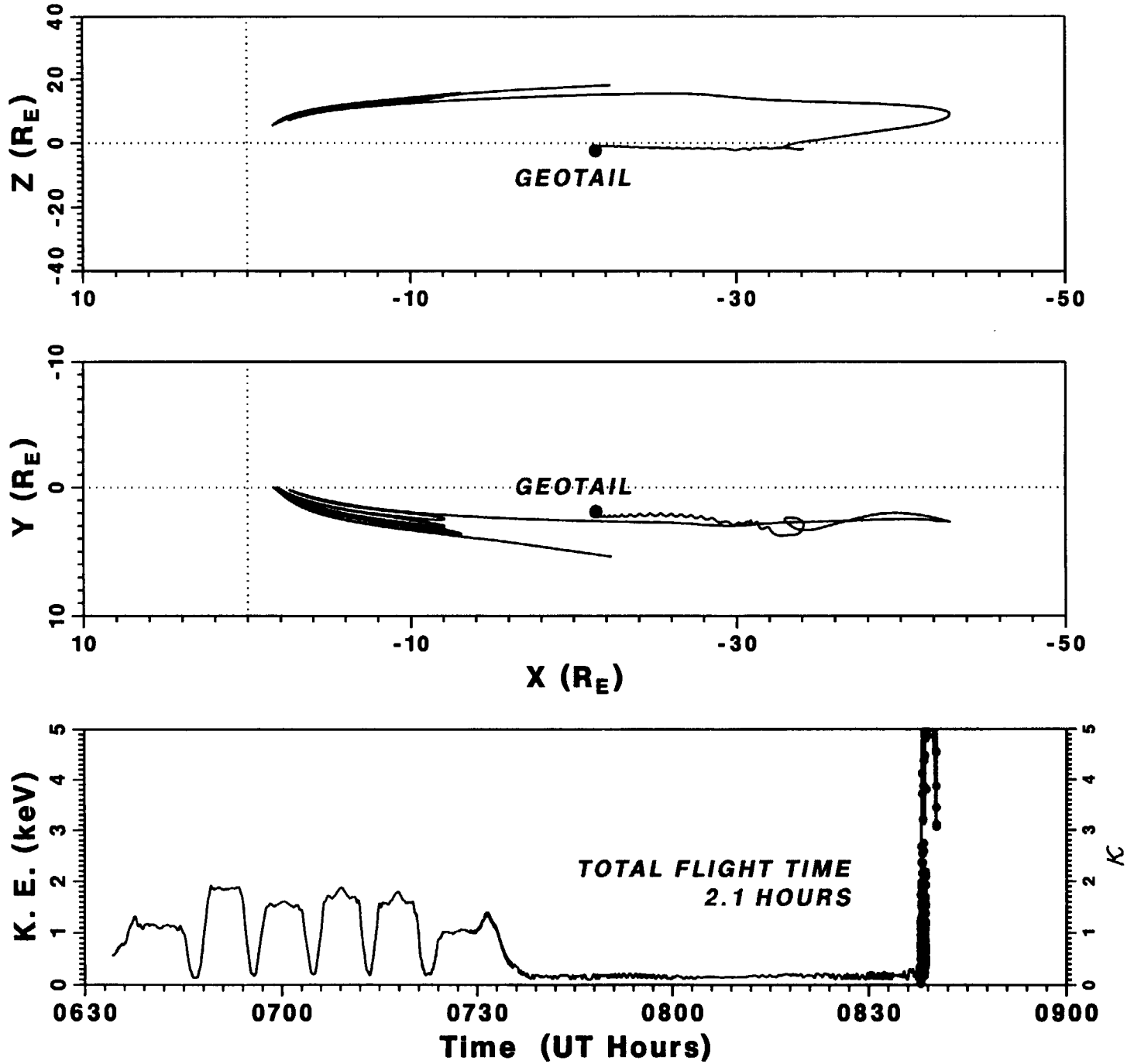

Figure 17